

See discussions, stats, and author profiles for this publication at: <https://www.researchgate.net/publication/281172310>

# Optimization of a Pretargeted Strategy for the PET Imaging of Colorectal Carcinoma via the Modulation of Radioligand Pharmacokinetics

ARTICLE *in* MOLECULAR PHARMACEUTICS · AUGUST 2015

Impact Factor: 4.38 · DOI: 10.1021/acs.molpharmaceut.5b00294 · Source: PubMed

---

CITATION

1

READS

34

---

## 8 AUTHORS, INCLUDING:



[Brian Zeglis](#)

City University of New York - Hunter College

46 PUBLICATIONS 1,281 CITATIONS

[SEE PROFILE](#)



[Christian Brand](#)

Memorial Sloan-Kettering Cancer Center

11 PUBLICATIONS 84 CITATIONS

[SEE PROFILE](#)



[Dalya Abdel-Atti](#)

Memorial Sloan-Kettering Cancer Center

8 PUBLICATIONS 23 CITATIONS

[SEE PROFILE](#)



[Sean Carlin](#)

Memorial Sloan-Kettering Cancer Center

51 PUBLICATIONS 989 CITATIONS

[SEE PROFILE](#)

# Optimization of a Pretargeted Strategy for the PET Imaging of Colorectal Carcinoma via the Modulation of Radioligand Pharmacokinetics

Brian M. Zeglis,<sup>\*,†</sup> Christian Brand,<sup>‡</sup> Dalya Abdel-Atti,<sup>‡</sup> Kathryn E. Carnazza,<sup>‡</sup> Brendon E. Cook,<sup>†</sup> Sean Carlin,<sup>‡</sup> Thomas Reiner,<sup>‡</sup> and Jason S. Lewis<sup>\*,‡,§</sup>

<sup>†</sup>Department of Chemistry and Biochemistry, Hunter College and the Graduate Center of the City University of New York, New York, New York 10021, United States

<sup>‡</sup>Department of Radiology, Memorial Sloan Kettering Cancer Center, New York, New York 10065, United States

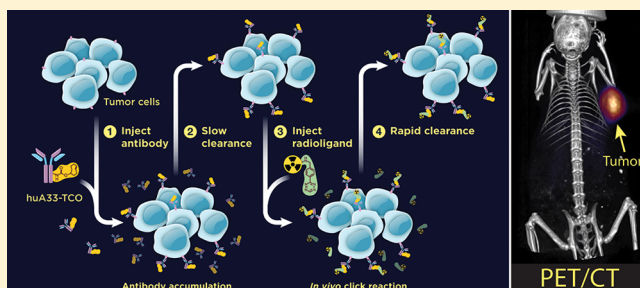
<sup>§</sup>Program in Molecular Pharmacology and Chemistry, Memorial Sloan Kettering Cancer Center, New York, New York 10065, United States

## Supporting Information

**ABSTRACT:** Pretargeted PET imaging has emerged as an effective strategy for merging the exquisite selectivity of antibody-based targeting vectors with the rapid pharmacokinetics of radiolabeled small molecules. We previously reported the development of a strategy for the pretargeted PET imaging of colorectal cancer based on the bioorthogonal inverse electron demand Diels–Alder reaction between a tetrazine-bearing radioligand and a transcyclotene-modified huA33 immunoconjugate. Although this method effectively delineated tumor tissue, its clinical potential was limited by the somewhat sluggish clearance of the radioligand through the gastrointestinal tract.

Herein, we report the development and *in vivo* validation of a pretargeted strategy for the PET imaging of colorectal carcinoma with dramatically improved pharmacokinetics. Two novel tetrazine constructs, Tz-PEG<sub>7</sub>-NOTA and Tz-SarAr, were synthesized, characterized, and radiolabeled with <sup>64</sup>Cu in high yield (>90%) and radiochemical purity (>99%). PET imaging and biodistribution experiments in healthy mice revealed that although <sup>64</sup>Cu-Tz-PEG<sub>7</sub>-NOTA is cleared via both the gastrointestinal and urinary tracts, <sup>64</sup>Cu-Tz-SarAr is rapidly excreted by the renal system alone. On this basis, <sup>64</sup>Cu-Tz-SarAr was selected for further *in vivo* evaluation. To this end, mice bearing A33 antigen-expressing SW1222 human colorectal carcinoma xenografts were administered huA33-TCO, and the immunoconjugate was given 24 h to accumulate at the tumor and clear from the blood, after which <sup>64</sup>Cu-Tz-SarAr was administered via intravenous tail vein injection. PET imaging and biodistribution experiments revealed specific uptake of the radiotracer in the tumor at early time points ( $5.6 \pm 0.7\% \text{ID/g}$  at 1 h p.i.), high tumor-to-background activity ratios, and rapid elimination of unclicked radioligand. Importantly, experiments with longer antibody accumulation intervals (48 and 120 h) yielded slight decreases in tumoral uptake but also concomitant increases in tumor-to-blood activity concentration ratios. This new strategy offers dosimetric benefits as well, yielding a total effective dose of 0.041 rem/mCi, far below the doses produced by directly labeled <sup>64</sup>Cu-NOTA-huA33 (0.133 rem/mCi) and <sup>89</sup>Zr-DFO-huA33 (1.54 rem/mCi). Ultimately, this pretargeted PET imaging strategy boasts a dramatically improved pharmacokinetic profile compared to our first generation system and is capable of clearly delineating tumor tissue with high image contrast at only a fraction of the radiation dose created by directly labeled radioimmunoconjugates.

**KEYWORDS:** Positron Emission Tomography, PET, Pretargeting, huA33, Colorectal Cancer, Click Chemistry, Inverse Electron Demand Diels–Alder Reaction, Tetrazine, Transcyclotene



## INTRODUCTION

Over the past 25 years, antibodies have emerged as extremely effective vectors for the sensitive and specific delivery of radioisotopes to tumors. A wide variety of radionuclides, ranging from <sup>124</sup>I for positron emission tomography (PET) to <sup>225</sup>Ac for targeted radiotherapy, have been conjugated to antibodies for preclinical investigations and, increasingly, clinical applications.<sup>1,2</sup> Yet despite the advent of radioimmunoconjugates, there remains

an important cause for concern regarding their ultimate clinical utility. Because of their size, intact IgG antibodies often have relatively long biological half-lives, requiring multiple days or even

Received: April 15, 2015

Revised: June 19, 2015

Accepted: August 19, 2015

weeks to reach their optimal biodistribution *in vivo*. In practice, this means that IgGs must necessarily be labeled with isotopes with long physical half-lives, such as  $^{89}\text{Zr}$  ( $t_{1/2} = 3.26$  d) for PET or  $^{177}\text{Lu}$  ( $t_{1/2} = 6.73$  d) for radiotherapy.<sup>3–5</sup> Although the resulting radioimmunoconjugates can deliver high concentrations of activity to tumor tissue, the long circulation times and radioactive half-lives often combine to produce significant—and potentially deleterious—radiation doses to healthy tissues as well.<sup>6</sup>

Given these concerns, a great deal of work has been dedicated to developing imaging agents that combine the specificity and affinity of full length IgGs with the rapid pharmacokinetics and favorable dosimetry of smaller molecules. Along these lines, one particularly popular strategy has been the development of radiopharmaceuticals based on truncated immunoglobulins, such as  $\text{F(ab')}_2$ ,  $\text{F(ab')}_1$ , and scFv fragments.<sup>7,8</sup> However, preclinical studies have shown that the smaller size and more rapid pharmacokinetics often come with a price: decreased activity concentrations in the targeted tissue and increased activity concentrations in excretory organs such as the kidneys.

An alternative approach for harnessing the affinity and specificity of intact IgGs while skirting their pharmacokinetic drawbacks lies in *pretargeting*.<sup>9–12</sup> Simply put, pretargeting strategies decouple the antibody from the radioactivity at the time of injection. First, an antibody that has been designed to bind both a target antigen and a radiolabeled hapten is injected into the blood. This antibody is then given time to accumulate at the tumor and concomitantly clear from the body. After this accumulation interval, a radiolabeled hapten is administered intravenously. This radioligand will then either bind to the antibody at the tumor or, due to its small size, clear rapidly from the body. In essence, the final radioimmunoconjugate is formed at the tumor itself. From a nuclear imaging perspective, the goal of these pretargeting methods is clear: to delineate tumor tissue at much earlier time points than traditional radioimmunoconjugates while significantly reducing the overall radiation burden to the patient, permitting safer and more accurate imaging over shorter time frames.

Until recently, three types of pretargeting technologies have dominated the literature: those based on (1) streptavidin-fused antibodies and biotin-based radioligands, (2) oligonucleotide-labeled antibodies and radioligands bearing complementary sequences, and (3) bispecific antibodies that bind both a target antigen and a radiolabeled hapten (e.g.,  $^{90}\text{Y}$ -DOTA).<sup>11,13–22</sup> Yet despite significant preclinical successes, the widespread application of each strategy has been hampered by its intrinsic limitations. For example, the immunogenicity of the streptavidin-bearing immunoconjugates has proven problematic in the clinic, and the inherent lack of modularity of bispecific antibodies is somewhat constraining as well.

In the past few years, a new type of pretargeting strategy based on the inverse electron demand Diels–Alder (IEDDA) reaction between tetrazine (Tz) and transcyclooctene (TCO) has emerged (Figure 1).<sup>23</sup> In 2008, the Fox laboratory brought the IEDDA cycloaddition back into the limelight as a click chemistry conjugation reaction after decades of quasi-obscurity as a favorite of physical organic chemists.<sup>24</sup> Since then, the reaction has been used for a wide variety of applications, including the fluorescent labeling of nanoparticles, antibodies, oligonucleotides, and small molecules, as well as the traditional synthesis of radiopharmaceuticals.<sup>25–35</sup> However, its greatest clinical impact may come as a tool for *in vivo* pretargeting. Indeed, it is almost perfectly suited for the task: the IEDDA reaction is extraordinarily rapid ( $k > 30,000 \text{ M}^{-1} \text{ s}^{-1}$ ), selective, robust, and, most importantly,

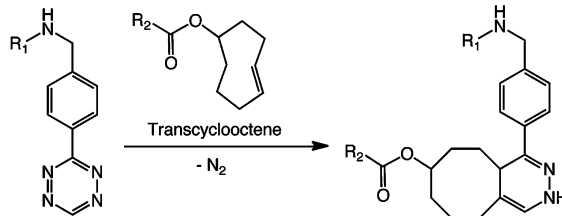


**Figure 1.** Inverse electron demand Diels–Alder cycloaddition.

bioorthogonal.<sup>36,37</sup> The use of IEDDA in pretargeting was pioneered largely by Rossin et al., who published an  $^{111}\text{In}$ -based SPECT imaging approach in 2010 and have followed this work with subsequent reports on the improvement of their systems using tetrazine-bearing clearing agents and more reactive dienophiles.<sup>38–40</sup> In addition, a number of other groups, including the laboratories of Weissleder and Carroll, have developed novel tetrazine-bearing radioligands for *in vivo* pretargeting.<sup>41–43</sup>

In 2013, our laboratory reported the development of a pretargeted PET imaging strategy based on the IEDDA reaction.<sup>44</sup> The system has two components—a TCO-modified conjugate of the colorectal cancer-targeting huA33 antibody (huA33-TCO) and a  $^{64}\text{Cu}$ -labeled tetrazine radioligand ( $^{64}\text{Cu}$ -Tz-NOTA)—and four steps: (1) injection of the huA33-TCO conjugate; (2) localization interval during which the antibody accumulates in the tumor and clears from the blood; (3) injection of the  $^{64}\text{Cu}$ -Tz-NOTA radioligand; and (4) *in vivo* click ligation of the two components, followed by the clearance of the excess radioligand (Figure 2). Critically, once bound to its glycoprotein antigen, the huA33 antibody remains on the surface of tumor cells, facilitating the subsequent *in vivo* ligation between its TCO cargo and the tetrazine-based radioligand. The methodology is highly effective, quickly and clearly delineating A33-antigen expressing SW1222 human colorectal cancer xenografts with high tumor-to-background activity ratios at a dose rate to healthy tissues far below traditional, directly labeled radioimmunoconjugates. However, there remained a stubborn obstacle to the clinical translation of this strategy for the staging, treatment planning, and treatment monitoring of colorectal carcinoma: the surplus unclicked  $^{64}\text{Cu}$ -Tz-NOTA radioligand is cleared somewhat sluggishly through the intestines. This is, of course, not an ideal situation for an imaging system for colorectal cancer. Therefore, to smooth the road from bench to bedside, we have sought to develop novel tetrazine radioligands with more favorable pharmacokinetic profiles.

Herein, we present the development and *in vivo* validation of an optimized strategy for the pretargeted PET imaging of colorectal carcinoma. To this end, we have synthesized, characterized, and studied the *in vivo* behavior of two novel  $^{64}\text{Cu}$ -labeled tetrazine radioligands possessing structural alterations geared toward the modulation of their pharmacokinetic profiles:  $^{64}\text{Cu}$ -Tz-PEG<sub>7</sub>-NOTA and  $^{64}\text{Cu}$ -Tz-SarAr. Our aim in creating these new radioligands was simple and straightforward: shifting the excretion of the tetrazine to the renal system, thereby accelerating its clearance from the body. Ultimately, we have found that a pretargeted PET imaging strategy based on the combination of huA33-TCO and  $^{64}\text{Cu}$ -Tz-SarAr marks a significant improvement over the first generation system, producing higher activity concentrations in the tumor and—due to the renal excretion of the novel radioligand—much improved tumor-to-background activity concentration ratios at early time points. Further, this optimized methodology represents a dosimetric improvement over the first generation system as well, producing

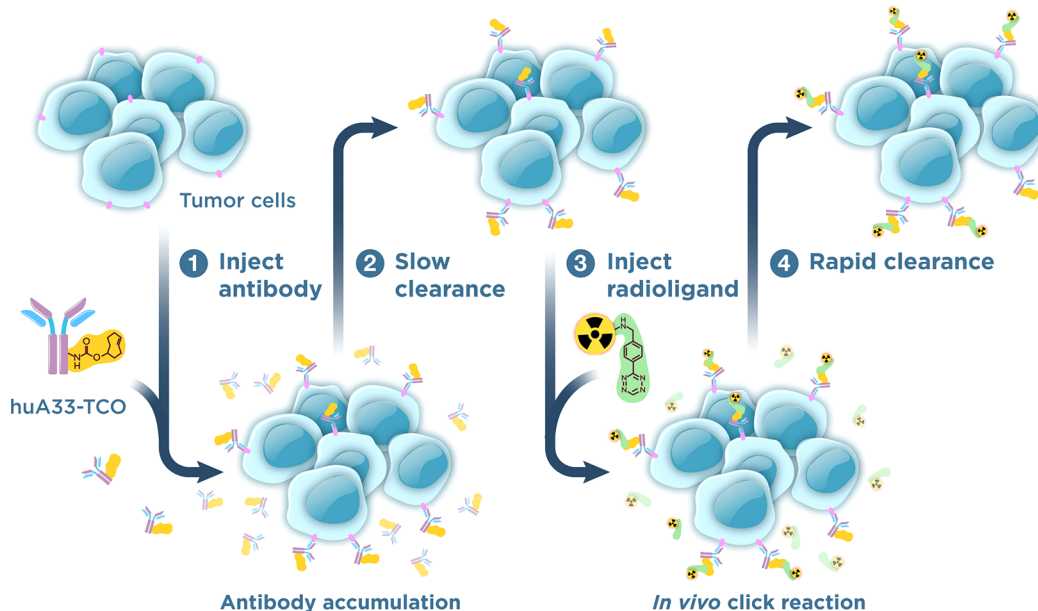


Figure 2. Schematic of the pretargeted PET imaging strategy.

dose rates far below those created by directly labeled radioimmunoconjugates.

## EXPERIMENTAL SECTION

**Methods and Materials.** Unless otherwise noted, all chemicals were acquired from Sigma-Aldrich (St. Louis, MO) and were used as received without further purification. All water employed was ultrapure ( $>18.2\text{ M}\Omega\text{cm}^{-1}$  at  $25^\circ\text{C}$ ), all DMSO was of molecular biology grade ( $>99.9\%$ ), and all other solvents were of the highest grade commercially available. Acetonitrile ( $\text{CH}_3\text{CN}$ ) and dimethylformamide (DMF) were purchased from Acros Organics (Waltham, MA) as extra dry over molecular sieves. Amine-reactive trans-cyclooctene [(*E*)-cyclooct-4-enyl 2,5-dioxo-1-pyrrolidinyl carbonate; TCO-NHS] and amine-reactive tetrazine (2,6-dioxo-1-pyrrolidinyl 5-[4-(1,2,4,5-tetrazin-3-yl)benzylamino]-5-oxopentanoate; Tz-NHS) were purchased from Sigma-Aldrich (St. Louis, MO). *p*-NCS-Bn-NOTA, *p*-NH<sub>2</sub>-Bn-NOTA, and DiAmSar chelators were purchased from Macrocyclics, Inc. (Dallas, TX). Tz-NOTA and <sup>64</sup>Cu-Tz-NOTA were synthesized as previously reported.<sup>44</sup> Humanized A33 (huA33) antibody was generously provided by the Ludwig Institute for Cancer Research (New York, NY) and stored at  $-80^\circ\text{C}$  prior to use. <sup>64</sup>Cu was purchased from Washington University, St. Louis, where it was produced on a medical cyclotron (Model CS-15, Cyclotron Corporation) via the <sup>64</sup>Ni-*(p,n)*<sup>64</sup>Cu transformation and purified as previously described to yield [<sup>64</sup>Cu]CuCl<sub>2</sub> with an effective specific activity of  $14,000 \pm 7,600\text{ mCi}/\mu\text{mol}$  ( $518 \pm 259\text{ GBq}/\mu\text{mol}$ ).<sup>45,46</sup> Human colorectal cancer cell line SW1222 was obtained from the Ludwig Institute for Cancer Immunotherapy and grown by serial passage. Amine-reactive AlexaFluor 680 (AF680-NHS) was purchased from ThermoFisher Scientific (Waltham, MA). All experiments using laboratory animals were performed according to a protocol approved by the Memorial Sloan Kettering Institutional Animal Care and Use Committee.

**Synthesis of tert-Butyl (1-(4-(1,2,4,5-Tetrazin-3-yl)-phenyl)-3,7-dioxo-11,14,17,20,23,26,29-heptaoxa-2,8-diazahentricontan-31-yl)carbamate (Tz-PEG<sub>7</sub>-NHBoc).** Tz-NHS (10 mg; 0.025 mmol; 398.4 g/mol) was dissolved in

400  $\mu\text{L}$  of DMSO and added to 15 mg *O*-(2-aminoethyl)-*O'*-(2-(bocamino)ethyl)hexaethylene glycol (0.032 mmol; 1.3 equiv; 468.6 g/mol). Ten microliters of triethylamine (7.3 mg; 0.072 mmol; 101.2 g/mol) was then added to this solution, and the solution was placed on an agitating thermomixer at 300 rpm for 30 min at room temperature. After 30 min, the reaction was purified via preparative C<sub>18</sub> HPLC using a gradient of 5:95 MeCN:H<sub>2</sub>O (both with 0.1% TFA) to 95:5 MeCN:H<sub>2</sub>O over 30 min ( $t_{\text{R}} = 18.2\text{ min}$ ). Lyophilization of the HPLC eluent yielded the purified product as 16 mg of a bright pink powder (MW = 751.9 g/mol; 0.021 mmol; 85% yield). <sup>1</sup>H NMR (500 MHz, DMSO) ppm:  $\delta$  10.52 (s, 1H), 8.50 (m, 3H), 7.82 (t, 1H), 7.46 (d, 2H), 6.69 (t, 1H), 4.33 (d, 2H), 3.42 (m, 22H), 3.33 (t, 2H), 3.31 (t, 2H), 3.12 (q, 2H), 2.99 (q, 2H), 2.12 (t, 2H), 2.03 (t, 2H), 2.12 (t, 2H), 1.70 (q, 2H), 1.29 (s, 9H). ESI-MS(+) *m/z* (%): 753.1 [M + H]<sup>+</sup>. HRMS (ESI) *m/z*: calcd for C<sub>35</sub>H<sub>57</sub>N<sub>11</sub>O<sub>11</sub>Na, 774.4005; found, 774.4014. UV-vis,  $\epsilon_{525}$ : 530 M<sup>-1</sup> cm<sup>-1</sup>.

**Synthesis of N<sup>1</sup>-(4-(1,2,4,5-Tetrazin-3-yl)benzyl)-N<sup>5</sup>-(23-amino-3,6,9,12,15,18,21-heptaoxatricosyl)glutaramide (Tz-PEG<sub>7</sub>-NH<sub>2</sub>).** Tz-PEG<sub>7</sub>-NHBoc (10 mg; 0.014 mmol; 717.5 g/mol) was dissolved in 400  $\mu\text{L}$  of 1:1 CH<sub>2</sub>Cl<sub>2</sub>:TFA and placed on an agitating thermomixer at 300 rpm for 30 min at room temperature. After 30 min, the solvent was removed via rotary evaporation, the residue was taken back up in H<sub>2</sub>O, and the reaction was purified via preparative C<sub>18</sub> HPLC using a gradient of 5:95 MeCN:H<sub>2</sub>O (both with 0.1% TFA) to 95:5 MeCN:H<sub>2</sub>O over 30 min ( $t_{\text{R}} = 12.5\text{ min}$ ). Lyophilization of the HPLC eluent yielded the purified product as 9 mg of a bright pink powder (MW = 651.7; 0.013 mmol; 95% yield). <sup>1</sup>H NMR (500 MHz, DMSO) ppm:  $\delta$  10.58 (s, 1H), 8.46 (m, 2H), 7.87 (t, 1H), 7.75 (d, 2H), 7.52 (d, 1H), 4.40 (d, 2H), 3.60–3.50 (m, 26H), 3.40 (t, 2H), 3.32 (bs, 2H), 3.20 (q, 2H), 2.99 (bs, 2H), 2.19 (t, 2H), 2.12 (t, 2H), 1.79 (q, 2H). ESI-MS(+) *m/z* (%): 652.9 [M + H]<sup>+</sup>. HRMS (ESI) *m/z*: calcd for C<sub>30</sub>H<sub>50</sub>N<sub>7</sub>O<sub>9</sub>, 652.3670; found, 652.3676. UV-vis,  $\epsilon_{525}$ : 535 M<sup>-1</sup> cm<sup>-1</sup>.

**Synthesis of 2,2',2''-(2-(4-(3-(1-(4-(1,2,4,5-Tetrazin-3-yl)phenyl)-3,7-dioxo-11,14,17,20,23,26,29-heptaoxa-2,8-diazahentricontan-31-yl)thioureido)benzyl)-1,4,7-triaxonane-1,4,7-triyl)triacetic Acid (Tz-PEG<sub>7</sub>-NOTA).**

Tz-PEG<sub>7</sub>-NH<sub>2</sub> (5 mg; 0.008 mmol; 651.8 g/mol) was dissolved in 400  $\mu$ L of DMSO and added to 10 mg of *p*-NCS-Bn-NOTA (0.022 mmol; 2.75 equiv; 450.5 g/mol). Ten microliters of triethylamine (7.3 mg; 0.072 mmol; 101.2 g/mol) was then added to this solution, and the solution was placed on an agitating thermomixer at 300 rpm for 30 min at room temperature. After 30 min, the reaction was purified via preparative C<sub>18</sub> HPLC using a gradient of 5:95 MeCN:H<sub>2</sub>O (both with 0.1% TFA) to 95:5 MeCN:H<sub>2</sub>O over 30 min ( $t_R$  = 15.5 min). Lyophilization of the HPLC eluent yielded the purified product as 6 mg of a bright pink powder (MW = 1102.2; 0.005 mmol; 68% yield). <sup>1</sup>H NMR (500 MHz, DMSO) ppm:  $\delta$  10.51 (s, 1H), 9.50 (bs, 1H), 8.40 (m, 3H), 7.79 (m, 1H), 7.62 (m, 1H), 7.47 (d, 2H), 7.35 (d, 2H), 7.03 (d, 2H), 4.43 (d, 2H), 4.00–3.20 (m, 50H), 3.12 (q, 2H), 2.96 (bs, 2H), 2.11 (t, 2H), 2.03 (t, 2H), 1.70 (q, 2H). ESI-MS(−) *m/z* (%): 1100.6 [M − H]<sup>−</sup>; 549.9 [M − 2H]<sup>2−</sup>. HRMS (ESI) *m/z*: calcd for C<sub>50</sub>H<sub>76</sub>N<sub>11</sub>O<sub>15</sub>S, 1102.5243; found, 1102.5253. UV-vis,  $\epsilon_{525}$ : 540 M<sup>−1</sup> cm<sup>−1</sup>.

**Synthesis of N<sup>1</sup>-(4-((Pivaloyloxy)amino)methyl)-benzyl)-3,6,10,13,16,19-hexaazabicyclo[6.6.6]icosane-1,8-diamine (SarAr-Bn-NHBoc).** N-Boc-4-(bromomethyl)-benzylamine (0.037 g; 0.12 mmol; 1.3 equiv; 300.2 g/mol) was added to a stirred solution of DiAmSar (0.030 g; 0.094 mmol; 1.0 equiv; 314.5 g/mol) in anhydrous dimethylformamide (4.0 mL) at room temperature. Sodium carbonate (0.034 g; 0.32 mmol; 3.5 equiv; 105.9 g/mol) was added, and the reaction solution was stirred at 70 °C for 16 h. The reaction was diluted with water (6.0 mL), and purification by HPLC (3.0 mL/min, 5 to 80% CH<sub>3</sub>CN in 15 min) afforded SarAr-Bn-NHBoc (MW = 533.8; 0.035 g; 70%) as a colorless solid ( $t_R$  = 9.4 min). <sup>1</sup>H NMR (500 MHz, DMSO) ppm:  $\delta$  7.38–7.50 (m, 4H), 4.18 (m, 2H), 2.31–3.98 (m, 42H), 1.35 (s, 9H). ESI-MS(+) *m/z*: 534.5 [M + H]<sup>+</sup>. HRMS (ESI) *m/z*: calcd for C<sub>27</sub>H<sub>52</sub>N<sub>9</sub>O<sub>2</sub>, 534.4244; found, 534.4250.

**Synthesis of N<sup>1</sup>-(4-(Aminomethyl)benzyl)-3,6,10,13,16,19-hexaazabicyclo[6.6.6]icosane-1,8-diamine (SarAr-Bn-NH<sub>2</sub>).** Trifluoroacetic acid (2.0 mL) was added slowly to a stirred solution of SarAr-Bn-NHBoc (0.031 g; 0.058 mmol; 1.0 equiv; 533.4 g/mol) in dry acetonitrile (2.0 mL), and the reaction mixture was stirred at room temperature for 90 min. Evaporation of the solvents under reduced pressure and purification by HPLC (6.0 mL/min, 5 to 60% CH<sub>3</sub>CN in 20 min) afforded SarAr-Bn-NH<sub>2</sub> (MW = 434.7; 0.026 g, 99%) as a colorless solid ( $t_R$  = 6.8 min). <sup>1</sup>H NMR (500 MHz, DMSO) ppm:  $\delta$  7.55 (d, 2H), 7.51 (d, 2H), 4.23 (s, 2H), 2.56–4.05 (m, 27H). ESI-MS(+) *m/z*: 434.4 [M + H]<sup>+</sup>. HRMS (ESI) *m/z*: calcd for C<sub>22</sub>H<sub>44</sub>N<sub>9</sub>, 434.3720; found, 434.3715.

**Synthesis of N<sup>1</sup>-(4-(1,2,4,5-Tetrazin-3-yl)benzyl)-N<sup>5</sup>-(4-((8-amino-3,6,10,13,16,19-hexaazabicyclo[6.6.6]icosan-1-yl)amino)methyl)benzyl)glutaramide (Tz-SarAr).** A solution of Tz-NHS (5.0 mg; 0.013 mmol; 1.0 equiv; 398.4 g/mol) in anhydrous dimethylformamide (400  $\mu$ L) was added to a stirred solution of SarAr-Bn-NH<sub>2</sub> (5.4 mg; 0.013 mmol; 1.0 equiv; 434.7 g/mol) in anhydrous dimethylformamide (200  $\mu$ L) at room temperature, and the reaction solution was stirred in the dark for 2 h at room temperature. After dilution with water (1.8 mL), purification by HPLC (1.0 mL/min, 5 to 80% CH<sub>3</sub>CN in 15 min) afforded Tz-SarAr (MW = 716.9; 3.9 mg; 42%) as a pink solid ( $t_R$  = 9.5 min). <sup>1</sup>H NMR (600 MHz, D<sub>2</sub>O) ppm:  $\delta$  10.25 (s, 1H), 8.31 (d, 2H), 7.46 (d, 2H), 7.22–7.27 (m, 4H), 4.39 (m, 2H), 4.24 (m, 3H), 2.46–3.95 (m, 24H), 2.41–2.44 (m, 4H), 1.83 (m, 2H). ESI-MS(+) *m/z*: 717.6

[M + H]<sup>+</sup>. HRMS (ESI) *m/z*: calcd for C<sub>36</sub>H<sub>57</sub>N<sub>14</sub>O<sub>2</sub>, 717.4789; found, 717.4788.

**Preparation of <sup>64</sup>Cu-Tz-PEG<sub>7</sub>-NOTA.** A solution of Tz-PEG<sub>7</sub>-NOTA (5–25  $\mu$ g; 4.5–22.6 nmol) in NH<sub>4</sub>OAc buffer (0.2 M, pH 5.5, 200  $\mu$ L) was first prepared. Then, the desired amount of <sup>64</sup>CuCl<sub>2</sub> in 0.1 M HCl (1500–7500  $\mu$ Ci) was added to the reaction mixture, and the solution was placed on an agitating thermomixer at 300 rpm for 30 min at room temperature. After this incubation, the <sup>64</sup>Cu-Tz-PEG<sub>7</sub>-NOTA was purified via reverse phase C<sub>18</sub> HPLC ( $t_R$  = 9.7 min) to yield the completed radioligand in >99% radionuclidian purity, 78 ± 6% decay-corrected isolated yield, and a specific activity of 278 ± 32  $\mu$ Ci/ $\mu$ g (323 ± 37 mCi/ $\mu$ mol; 11.9 ± 1.3 GBq/ $\mu$ mol).

**Preparation of <sup>64</sup>Cu-Tz-SarAr.** A solution of Tz-SarAr (5–25  $\mu$ g; 6.9–34.9 nmol) in NH<sub>4</sub>OAc buffer (0.2 M, pH 5.5, 200  $\mu$ L) was first prepared. Then, the desired amount of <sup>64</sup>CuCl<sub>2</sub> in 0.1 M HCl (1500–7500  $\mu$ Ci) was added to the reaction mixture, and the solution was placed on an agitating thermomixer at 300 rpm for 30 min at room temperature. After this incubation, the <sup>64</sup>Cu-Tz-SarAr was purified via reverse phase C<sub>18</sub> HPLC ( $t_R$  = 8.7 min) to yield the completed radioligand in >99% radio-nuclidian purity, 79 ± 7% decay-corrected isolated yield, and a specific activity of 398 ± 46  $\mu$ Ci/ $\mu$ g (310 ± 36 mCi/ $\mu$ mol; 11.5 ± 1.3 GBq/ $\mu$ mol) (*n* = 6).

**Pretargeted PET Imaging Experiments.** All pretargeted PET imaging experiments were performed on an Inveon PET/CT scanner (Siemens Healthcare Global). Female athymic nude mice (*n* = 5 per radioligand) bearing subcutaneous SW1222 (right shoulder) xenografts (100–150 mm<sup>3</sup>, 9–12 days post-inoculation) were administered 100  $\mu$ g (0.66 nmol) of huA33-TCO (in 200  $\mu$ L of 0.9% sterile saline) via intravenous tail vein injection. After an accumulation interval of 24, 48, or 120 h, the same mice were then administered either <sup>64</sup>Cu-Tz-PEG<sub>7</sub>-NOTA or <sup>64</sup>Cu-Tz-SarAr (400–450  $\mu$ Ci in 200  $\mu$ L of 0.9% sterile saline), also via intravenous tail vein injection (*t* = 0). For both <sup>64</sup>Cu-Tz-PEG<sub>7</sub>-NOTA and <sup>64</sup>Cu-Tz-SarAr, the specific activity of the radiotracer was adjusted using cold <sup>nat</sup>Cu-Tz-PEG<sub>7</sub>-NOTA or <sup>nat</sup>Cu-Tz-SarAr such that the molar ratio of Tz<sub>Injected</sub>:huA33<sub>Injected</sub> ≈ 1:1. Approximately 5 min prior to the PET images, mice were anesthetized by inhalation of a 2% isoflurane (Baxter Healthcare, Deerfield, IL) oxygen gas mixture and placed on the scanner bed; anesthesia was maintained using a 1% isoflurane gas mixture. Static scans were recorded at various time points after injection with a minimum of 30 million coincident events (10–30 min total scan time). An energy window of 350–700 keV and a coincidence timing window of 6 ns were used. Data were sorted into 2-dimensional histograms by Fourier rebinning, and the images were reconstructed using a two-dimensional ordered subset expectation maximization (2DOSEM) algorithm (16 subsets, 4 iterations) into a 128 × 128 × 159 (0.78 × 0.78 × 0.80 mm) matrix. The image data was normalized to correct for non-uniformity of response of the PET, dead-time count losses, positron branching ratio, and physical decay to the time of injection, but no attenuation, scatter, or partial-volume averaging correction was applied. Activity concentrations (percentage of dose per gram of tissue [%ID/g]) and maximum intensity projections were determined by conversion of the counting rates from the reconstructed images. All of the resulting PET images were analyzed using ASIPro VM software. Whole-body CT scans were acquired with a voltage of 80 kV and 500  $\mu$ A. One hundred and twenty rotational steps for a total of 220° were acquired with a total scan time of 120 s and 145 ms per frame exposure. Combined PET/CT images were processed using Inveon Research Workplace software.

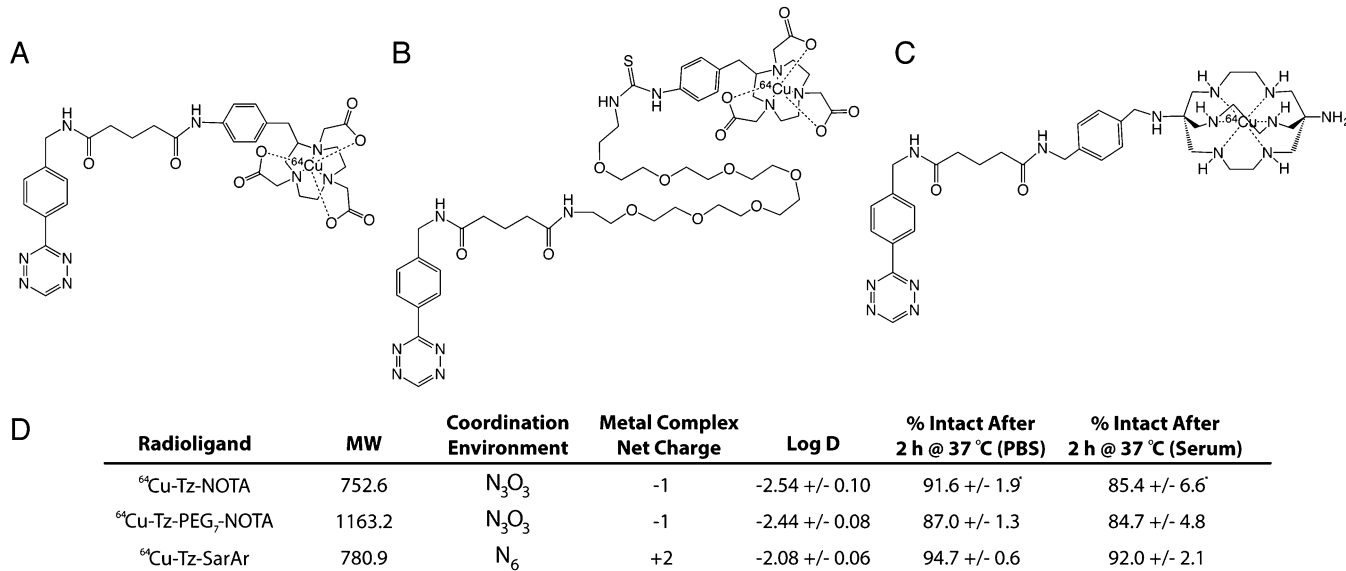


**Figure 3.** Structures of (A) <sup>64</sup>Cu-Tz-NOTA, (B) <sup>64</sup>Cu-Tz-PEG<sub>7</sub>-NOTA, (C) <sup>64</sup>Cu-Tz-SarAr, along with (D) some selected properties of the three tetrazine radioligands. Data originally reported in Zeglis, B. M. et al. *Journal of Nuclear Medicine*. **54**, 1389–1396 (2013). ©2013 by the Society of Nuclear Medicine and Molecular Imaging, Inc.<sup>44</sup>

**Pretargeted Biodistribution Experiments.** Female athymic nude mice bearing subcutaneous SW1222 (right shoulder) xenografts (100–150 mm<sup>3</sup>, 18–21 days postinoculation) were administered 100 µg (0.66 nmol) of huA33-TCO (in 200 µL of 0.9% sterile saline) via intravenous tail vein injection. After an accumulation interval period of 24, 48, or 120 h, the same mice were then administered <sup>64</sup>Cu-Tz-SarAr (300–350 µCi in 200 µL of 0.9% sterile saline), also via intravenous tail vein injection (*t*=0). As in the PET imaging experiments, the specific activity of the radiotracer was adjusted using cold <sup>nat</sup>Cu-Tz-SarAr such that the molar ratio of Tz<sub>injected</sub>:huA33<sub>injected</sub> = 1:1. Animals (*n* = 4 per group) were euthanized by CO<sub>2</sub>(g) asphyxiation at 1, 4, 12, and 24 h after injection. After asphyxiation, tissues were removed, rinsed in water, dried in air for 5 min, weighed, and counted in a gamma counter calibrated for <sup>64</sup>Cu. Counts were converted to activity using a calibration curve generated from known standards. Count data were background- and decay-corrected to the time of injection, and the percent injected dose per gram (%ID/g) for each tissue sample was calculated by normalization to the total activity injected.

## RESULTS AND DISCUSSION

**System Design.** On the most basic level, this strategy relies on three components—the antibody, the transcyclooctene, and the tetrazine—and therefore, thoughtful consideration of each is critical. HuA33 is a humanized antibody that targets the A33 antigen, a transmembrane glycoprotein abundantly expressed by >95% of all colorectal cancer tumors.<sup>47</sup> Although low levels of expression of the A33 antigen have been found on normal bowel epithelium, clinical studies with <sup>124</sup>I-labeled huA33 have illustrated that tumor tissue retains the antibody far longer than healthy epithelium, making this antigen ripe for a pretargeted approach.<sup>47–51</sup> Further, in vitro studies have shown that the huA33-A33 antigen complex persists on the surface of the cell for days after formation.<sup>52</sup> This is critical for pretargeting methodologies, as the antibody must remain accessible to the radioligand for the in vivo ligation to occur. For the transcyclooctene and tetrazine components, we have employed transcyclooct-4-en-1-yl

hydrogen carbonate (TCO) and 3-(benzylamine)-1,2,4,5-tetrazine (Tz). The IEDDA cycloaddition between these two moieties has been shown to be extraordinarily rapid with a second order rate constant of >30,000 M<sup>-1</sup> s<sup>-1</sup>.<sup>36</sup> Furthermore, both components have been shown to be sufficiently stable in physiological settings, and conveniently, amine-reactive variants (TCO-NHS and Tz-NHS) of both are commercially available.

Delving deeper, the core of this investigation lies in the redesign of the <sup>64</sup>Cu-labeled Tz radioligand. Although our first generation pretargeting methodology proved effective at delineating tumor tissue, the relatively slow clearance (*t*<sub>1/2</sub> ~ 4 h) of the <sup>64</sup>Cu-Tz-NOTA (Figure 3A) through the intestinal tract understandably dampened enthusiasm for its clinical translation as a methodology for imaging colorectal cancer. As a result, we sought to create two novel <sup>64</sup>Cu-Tz radioligands with structural alterations geared at improving their pharmacokinetic profiles. To accomplish this goal, we turned to two different structural motifs that have been shown to exert significant influence on the *in vivo* behavior of radiotracers: polyethylene glycol (PEG) linkers and chelators. A substantial body of literature exists detailing the ability of PEG linkers—or probably more aptly, oligo-ethylene glycol linkers—to accelerate the clearance and lower the nontarget tissue uptake of radiopharmaceuticals.<sup>53–58</sup> Likewise, for agents labeled with metallic isotopes, there are also a number of studies illustrating that changes to the identity of the chelator, and consequently the overall charge of the radiometal–chelator complex, can dramatically influence pharmacokinetics as well.<sup>59–64</sup> Armed with this information, we designed two novel <sup>64</sup>Cu-labeled Tz radioligands. In the first, <sup>64</sup>Cu-Tz-PEG<sub>7</sub>-NOTA, a PEG<sub>7</sub> spacer separates the tetrazine moiety from the NOTA chelator (Figure 3B). In the second, <sup>64</sup>Cu-Tz-SarAr, a sarcophagine-based chelator (SarAr) replaces the NOTA macrocycle, not only changing the coordination environment from N<sub>3</sub>O<sub>3</sub> to N<sub>6</sub> but, more importantly, shifting the overall charge of the metal–ligand complex from -1 (Cu<sup>II</sup>–NOTA) to +2 (Cu<sup>II</sup>–SarAr) (Figure 3C,D).

**Synthesis and Characterization.** The first step in the investigation was the synthesis of the molecular components of the pretargeting system. Tz-PEG<sub>7</sub>-NOTA was synthesized in

49% yield over three facile steps: the coupling of Tz-NHS and monofunctional O-(2-aminoethyl)-O'-[2-(bocamino)ethyl]-hexaethylene glycol to form Tz-PEG<sub>7</sub>-NHBoc, the removal of the *tert*-butyloxycarbonyl protecting group with TFA/CH<sub>2</sub>Cl<sub>2</sub>, and the coupling of Tz-PEG<sub>7</sub>-NH<sub>2</sub> with *p*-NCS-Bn-NOTA (Figure S1). Given the symmetry of its sarcophagine precursor, Tz-SarAr required a slightly more careful synthesis. In this case, the monoalkylation of DiAmSar with Boc-protected 4-(bromomethyl)-benzylamine was followed by the removal of the acid-labile protecting group with TFA and the coupling of the resulting SarAr-Bn-NH<sub>2</sub> moiety with Tz-NHS to produce the final product in 29% yield over three steps (Figure S2). For both syntheses, all intermediates as well as the completed tetrazine-bearing precursors were analyzed and purified using reverse-phase C<sub>18</sub> HPLC and characterized via UV-vis spectrophotometry, <sup>1</sup>H NMR, ESI-MS, and high-resolution mass spectrometry (Supporting Methods).

Once the precursors were in hand, the tetrazine constructs were then radiolabeled via incubation with [<sup>64</sup>Cu]-CuCl<sub>2</sub> for 10 min at room temperature in 200 mM NH<sub>4</sub>OAc, pH 5.0 and purified via reverse-phase C<sub>18</sub> HPLC (*t*<sub>R</sub> = 8.7 min for <sup>64</sup>Cu-Tz-SarAr and 9.7 min for <sup>64</sup>Cu-Tz-PEG<sub>7</sub>-NOTA; Supporting Methods and Figures S3–S6). In both cases, the identity of the radiolabeled product was confirmed via coinjection of unlabeled <sup>nat</sup>Cu-Tz-SarAr and <sup>nat</sup>Cu-Tz-PEG<sub>7</sub>-NOTA standards. Ultimately, <sup>64</sup>Cu-Tz-PEG<sub>7</sub>-NOTA was prepared in >99% radionuclidic purity, 78 ± 6% decay-corrected isolated yield, and a specific activity of 323 ± 37 mCi/μmol (11.9 ± 1.3 GBq/μmol; *n* = 6). Similarly, <sup>64</sup>Cu-Tz-SarAr was synthesized in >99% radionuclidic purity, 79 ± 7% decay-corrected isolated yield, and a specific activity of 310 ± 36 mCi/μmol (11.5 ± 1.3 GBq/μmol; *n* = 6). The first generation <sup>64</sup>Cu-Tz-NOTA radioligand was synthesized, radiolabeled, and purified as previously reported.<sup>44</sup> To probe the influence of the structural changes on solubility, we determined the partition coefficients of the various radioligands using PBS (pH 7.4) and 1-octanol (Supporting Methods and Table S1). Although all three radioligands proved reasonably hydrophilic, with logD values below −2, some interesting differences were observed nonetheless. For example, the replacement of NOTA with SarAr rendered <sup>64</sup>Cu-Tz-SarAr (logD = −2.08 ± 0.06) more hydrophobic than <sup>64</sup>Cu-Tz-NOTA (logD = −2.54 ± 0.1). Further, the addition of the PEG<sub>7</sub> moiety in <sup>64</sup>Cu-Tz-PEG<sub>7</sub>-NOTA surprisingly does not leave the product more hydrophilic (logD = −2.44 ± 0.08) than its linker-lacking cousin.

Next, the aqueous and serum stabilities were determined via incubation at 37 °C (Tables S2 and S3). Both <sup>64</sup>Cu-Tz-PEG<sub>7</sub>-NOTA and <sup>64</sup>Cu-Tz-SarAr were shown to be fairly stable in PBS (pH 7.4). It was determined that 94.7 ± 0.6% and 93.3 ± 0.5% of <sup>64</sup>Cu-Tz-SarAr remained intact after 2 and 4 h,<sup>59,60</sup> respectively. <sup>64</sup>Cu-Tz-PEG<sub>7</sub>-NOTA proved similarly stable with 87.0 ± 1.3% (2 h) and 83.2 ± 4.6% (4 h) intact. Not surprisingly, more extensive decomposition was observed in human serum. For example, after a 4 h incubation, 77.8 ± 3.5% and 81.2 ± 3.7% of <sup>64</sup>Cu-Tz-PEG<sub>7</sub>-NOTA and <sup>64</sup>Cu-Tz-SarAr, respectively, remained intact. In all cases, the decomposition of the radioligands resulted in the creation of a poorly resolved array of more hydrophilic catabolites that elute at earlier time points (e.g., 6–8 min). Critically, however, neither the release of <sup>64</sup>Cu<sup>2+</sup> from the chelators nor the binding of significant amounts of the radioligands to serum proteins was observed in any of the trials. These results are generally consistent with those previously obtained for <sup>64</sup>Cu-Tz-NOTA, a reasonable result given that the

radio-HPLC analysis suggests that the decomposition is related primarily to the breakdown of the tetrazine and all three constructs bear identical tetrazine moieties. Ultimately, although it may be tempting to become concerned with these rates of decomposition, it is important to remember that between the short blood half-lives of these small molecules and the exceptional speed of the IEDDA reaction, it is extremely unlikely that the decomposition of the radioligands will severely impair their chances of functioning *in vivo*.

Finally, huA33-TCO was synthesized via the coupling of TCO-NHS to the huA33 antibody as previously described (Supporting Methods and Figure S7).<sup>44</sup> Briefly, a solution of huA33 (2–3 mg/mL) in PBS was adjusted to pH 8.8–9.0 with 0.1 M Na<sub>2</sub>CO<sub>3</sub>. Ten molar equivalents of TCO-NHS were then added to the antibody solution, and the resulting reaction mixture was incubated at room temperature for 1 h prior to purification via size exclusion chromatography. Using a fluorophore-labeled tetrazine probe (Tz-PEG<sub>7</sub>-AF680), the TCO occupancy of the huA33 was determined to be 3.6 ± 0.6 TCO/mAb, a result consistent with the values obtained in our previous investigation (Supporting Methods).<sup>44,65</sup> Both <sup>64</sup>Cu-Tz-PEG<sub>7</sub>-NOTA and <sup>64</sup>Cu-Tz-SarAr were incubated with huA33-TCO, rapidly resulting in >95% reaction yields and, after purification, <sup>64</sup>Cu-labeled huA33 radioimmunoconjugates with high specific activities (>2 mCi/mg; >74 MBq/mg) and immunoreactive fractions (>0.95) with A33 antigen-expressing SW1222 human colorectal carcinoma cells (Methods and Table S4). Importantly, control reactions between unmodified huA33 and the <sup>64</sup>Cu-labeled tetrazines as well as huA33-TCO and uncomplexed <sup>64</sup>Cu<sup>2+</sup> resulted in <1% radiolabeling of the huA33 constructs.

**In Vivo Evaluation of the <sup>64</sup>Cu-Labeled Tetrazines.** The next step of the investigation was the study of the *in vivo* behavior and pharmacokinetics of the <sup>64</sup>Cu-labeled tetrazine radioligands. To this end, acute biodistribution and PET imaging experiments were performed in healthy athymic nude mice injected with <sup>64</sup>Cu-Tz-NOTA, <sup>64</sup>Cu-Tz-PEG<sub>7</sub>-NOTA, or <sup>64</sup>Cu-Tz-SarAr (Figure 4 and Supporting Methods, Figures S8–S10, and Tables S5–S7). Critically, all three <sup>64</sup>Cu-labeled tetrazines accumulate very little in most healthy nontarget tissues with activity concentrations lower, often significantly, than 0.5 %ID/g beyond the earliest time points. Indeed, the largest differences between the three radioligands lie in their excretion. As we discussed in our previous report, the first generation <sup>64</sup>Cu-Tz-NOTA is excreted relatively slowly through the feces with 10.0 ± 1.3 %ID/g remaining in the large intestine and its contents at 4 h p.i., a number which dips to 1.4 ± 0.7 %ID/g at 24 h. The addition of the PEG linker in <sup>64</sup>Cu-Tz-PEG<sub>7</sub>-NOTA noticeably changes things in two ways. First, the elimination of the radioligand through the gut is accelerated with only 4.9 ± 0.7 %ID/g in the large intestine and its contents at 4 h p.i. Second, it appears that some of the excretion of the radiotracer has been shifted to the urinary tract, as the kidneys display activity concentrations of 1.5 ± 0.2 %ID/g and 1.2 ± 0.4 %ID/g at 1 and 4 h, respectively. However, the largest shift of all is observed with <sup>64</sup>Cu-Tz-SarAr. In this case, the radioligand is excreted exclusively and rapidly through the renal system. To wit, the tissue with the highest levels of <sup>64</sup>Cu-Tz-SarAr at 1 h p.i. is the kidney with only 2.3 ± 0.4 %ID/g. The activity in the kidneys clears with time, but even at 24 h, some retention of the radioligand is evident. Complementary PET imaging experiments confirmed the observations from the biodistributions: <sup>64</sup>Cu-Tz-SarAr clears quickly and cleanly through the urinary tract, <sup>64</sup>Cu-Tz-NOTA is eliminated somewhat sluggishly through the

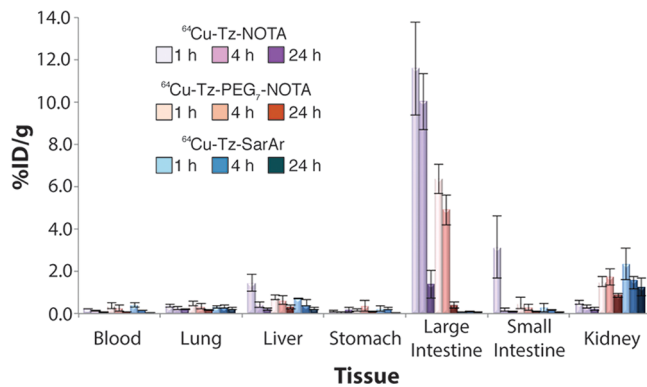


**Figure 4.** Biodistribution data (%ID/g  $\pm$  SD) of <sup>64</sup>Cu-Tz-NOTA, <sup>64</sup>Cu-Tz-PEG<sub>7</sub>-NOTA, and <sup>64</sup>Cu-Tz-SarAr in healthy athymic nude mice ( $n = 4$  for each time point). Mice were administered the radioligands (25–30  $\mu$ Ci in 200  $\mu$ L of 0.9% sterile saline) via intravenous tail vein injection and euthanized by CO<sub>2</sub>(g) asphyxiation at 1, 4, and 24 h after injection.

gastrointestinal pathway, and <sup>64</sup>Cu-Tz-PEG<sub>7</sub>-NOTA represents an intermediate case with excretion through both the intestines and the kidneys.

As we discussed in our original report, the gastrointestinal elimination of <sup>64</sup>Cu-Tz-NOTA is somewhat surprising, especially considering its relatively low molecular weight. Generally speaking, pharmacokinetic profiles are notoriously complicated phenomena, and thus any attempt to explain the shifts in excretion pathways that have been observed risks degenerating into base conjecture. That said, it is unlikely that changes in the hydrophobicity of the radioligands are responsible. As we have seen, <sup>64</sup>Cu-Tz-SarAr ( $\log D = -2.08 \pm 0.06$ ) is actually more hydrophobic than <sup>64</sup>Cu-Tz-NOTA ( $\log D = -2.54 \pm 0.1$ ) and <sup>64</sup>Cu-Tz-PEG<sub>7</sub>-NOTA ( $\log D = -2.44 \pm 0.08$ ), a trait that is seldom associated with increased renal elimination. More likely explanations for the shifts in pharmacokinetics may lie in the

changes to the chelator and overall net charge of the radioligands: from NOTA and a  $-1$  overall net charge to SarAr and a  $+2$  overall net charge. A number of laboratories have reported that changing the chelator in a radiopharmaceutical can have dramatic effects on the biodistribution of the imaging agent.<sup>59–61,63,64,66</sup> In addition, there is also ample data illustrating that the introduction of positive charge to a radiopharmaceutical can increase renal clearance and kidney retention.<sup>62,67,68</sup> Clearly, however, more than one factor is in play here, as <sup>64</sup>Cu-Tz-NOTA possesses a pharmacokinetic profile that differs from those of both <sup>64</sup>Cu-Tz-PEG<sub>7</sub>-NOTA (with which it shares a chelator) and <sup>64</sup>Cu-Tz-SarAr. Most likely of all, yet perhaps least satisfying to those searching for a simple answer, is that the differences in pharmacokinetics observed for the three radioligands are the result of the complex interplay of a variety of factors, including but not limited to hydrophobicity, charge, protein binding affinity, and molecular structure.

Specifics aside, these data ultimately made our choice easy: <sup>64</sup>Cu-Tz-SarAr clearly possesses the most promising elimination pharmacokinetics for our pretargeted PET imaging strategy. Simply put, the radioligand is excreted rapidly via the bladder and kidneys, and the activity concentrations in the large intestine, a critical source of background noise in clinical colorectal cancer imaging, remains remarkably low (e.g.,  $0.07 \pm 0.01$  %ID/g at 1 h p.i.). Additional experiments were conducted to interrogate the in vivo performance of <sup>64</sup>Cu-Tz-SarAr further. Blood activity measurements, for example, revealed that the vast majority of the radioligand clears from the blood with a residence time of  $\sim 16$  min (Table S8 and Figure S11). Moreover, in vivo stability assays indicate that  $96.8 \pm 0.8\%$  of the <sup>64</sup>Cu-Tz-SarAr remains intact at 15 min postinjection, a value which falls to  $82.0 \pm 3.3\%$  at 1 h p.i. and ultimately  $29.0 \pm 5.9\%$  4 h after administration (Table S9). These numbers clearly indicate that although <sup>64</sup>Cu-Tz-SarAr is not tremendously stable in vivo, the radioligand unquestionably remains intact during the critical initial blood residence time frame.

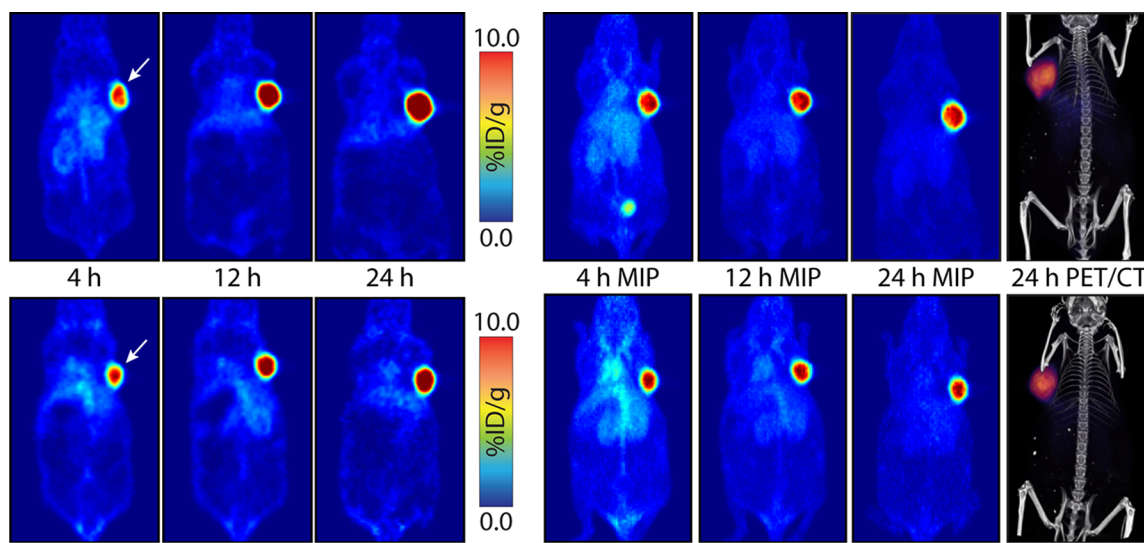


**Figure 5.** Pretargeted PET imaging using <sup>64</sup>Cu-Tz-SarAr and a 24 h accumulation interval. Female athymic nude mice ( $n = 5$ ) bearing subcutaneous SW1222 (right shoulder) xenografts (100–150 mm<sup>3</sup>, 18–21 days postinoculation) were administered 100  $\mu$ g (0.66 nmol) of huA33-TCO (in 200  $\mu$ L of 0.9% sterile saline) via intravenous tail vein injection. After an accumulation interval of 24 h, the same mice were then administered <sup>64</sup>Cu-Tz-SarAr (400–450  $\mu$ Ci, 0.66–0.77 nmol, in 200  $\mu$ L of 0.9% sterile saline) also via intravenous tail vein injection ( $t = 0$ ). The coronal slices (left) intersect the center of the tumor (white arrow). Maximum intensity projections (MIP) at 4, 12, and 24 h postinjection are also displayed (right) along with coregistered PET/CT images collected at 24 h p.i. (far right, perspective flipped).

**In Vivo Pretargeting.** Because of its promising pharmacokinetic profile,  $^{64}\text{Cu}$ -Tz-SarAr was selected for further in vivo pretargeting experiments. (Notably, however, successful pretargeted PET imaging experiments were performed with  $^{64}\text{Cu}$ -Tz-PEG<sub>7</sub>-NOTA (see Figure S12). To this end, athymic nude mice bearing A33 antigen-expressing SW1222 human colorectal carcinoma tumors were first injected with huA33-TCO (100  $\mu\text{g}$ ). After a 24 h interval during which huA33-TCO accumulates in the tumor and clears from the blood, the mice were injected with  $^{64}\text{Cu}$ -Tz-SarAr (400–450  $\mu\text{Ci}$ ). Importantly, the specific activity of the radiotracer was adjusted using cold  $^{nat}\text{Cu}$ -Tz-SarAr such that the molar ratio of Tz-SarAr:huA33-TCO was approximately 1:1, a value that both pilot experiments and previously published reports implied would yield the optimal results.<sup>38,40,44</sup> Both the PET imaging (Figure 5 and Figure S13) and biodistribution results (Table 1 and Tables S10 and S11) indicate that the

**Table 1. Biodistribution Data for in Vivo Pretargeting Experiment Using  $^{64}\text{Cu}$ -Tz-SarAr and a 24 h Accumulation Interval**

	1 h	4 h	12 h	24 h
blood	$4.20 \pm 0.80^a$	$4.00 \pm 0.37$	$2.19 \pm 0.39$	$2.61 \pm 0.20$
tumor	$5.63 \pm 0.67$	$5.56 \pm 0.91$	$6.74 \pm 1.26$	$7.38 \pm 2.02$
heart	$1.81 \pm 0.46$	$1.45 \pm 0.03$	$0.84 \pm 0.10$	$0.81 \pm 0.04$
lung	$1.65 \pm 0.51$	$1.55 \pm 0.45$	$1.24 \pm 0.22$	$0.99 \pm 0.24$
liver	$1.60 \pm 0.12$	$1.45 \pm 0.21$	$1.33 \pm 0.53$	$1.51 \pm 0.20$
spleen	$0.98 \pm 0.25$	$0.81 \pm 0.20$	$0.65 \pm 0.17$	$0.64 \pm 0.04$
stomach	$0.73 \pm 0.19$	$0.56 \pm 0.20$	$0.21 \pm 0.10$	$0.28 \pm 0.07$
large intestine	$0.21 \pm 0.09$	$0.48 \pm 0.09$	$0.20 \pm 0.04$	$0.26 \pm 0.06$
small intestine	$0.88 \pm 0.09$	$0.62 \pm 0.06$	$0.35 \pm 0.08$	$0.45 \pm 0.07$
kidney	$3.08 \pm 0.28$	$2.77 \pm 0.57$	$1.87 \pm 0.42$	$2.00 \pm 0.24$
muscle	$0.38 \pm 0.06$	$0.37 \pm 0.07$	$0.15 \pm 0.01$	$0.20 \pm 0.07$
bone	$0.67 \pm 0.14$	$0.34 \pm 0.18$	$0.23 \pm 0.05$	$0.29 \pm 0.05$

<sup>a</sup>Values are %ID/g  $\pm$  SD. Mice ( $n = 4$ ) bearing subcutaneous SW1222 xenografts were administered huA33-TCO via tail vein injection. After 24 h, the same mice were administered  $^{64}\text{Cu}$ -Tz-SarAr, also via tail vein injection. Stomach, small intestine, and large intestine values include contents.

strategy quickly and clearly delineates colorectal carcinoma tissue with low activity concentrations in nontarget tissues. Even at just 1 h postinjection, the activity concentration in the tumor ( $5.6 \pm 0.7$  %ID/g) is the highest of all tissues surveyed, whereas the blood ( $4.2 \pm 0.8$  %ID/g) and kidneys ( $3.1 \pm 0.3$  %ID/g) stand as the healthy organs with the highest background activity concentrations. Critically, over the course of the experiment, the activity in the nontarget tissues clears. For example, at 12 h postinjection, the activity concentration in the blood and kidneys is reduced to  $2.2 \pm 0.4$  %ID/g and  $1.9 \pm 0.4$  %ID/g, respectively, while the tumoral activity concentration at the same time point is  $6.7 \pm 1.3$  %ID/g. Further, at these later time points, all other nontarget tissues contain  $<1.5$  %ID/g. Even at early time points, the tumor-to-background activity ratios are favorable (e.g., tumor:muscle =  $14.9 \pm 2.9$  at 1 h p.i.), and these values grow with time, ultimately reaching  $45.1 \pm 8.5$  at 12 h and  $37.37 \pm 16.1$  at 24 h (Table S11). Notably, control PET imaging experiments were run using  $^{64}\text{Cu}$ -Tz-SarAr alone as well as  $^{64}\text{Cu}$ -Tz-SarAr with unmodified huA33, and both cases resulted in minimal ( $<0.5$  %ID/g) uptake in the tumor.

On the whole, both the PET imaging and biodistribution data compare very favorably with the results obtained for the first generation  $^{64}\text{Cu}$ -Tz-NOTA system (Figure S13 and

Tables S12 and 13). The activity concentrations in the tumor, for example, are slightly higher using the  $^{64}\text{Cu}$ -Tz-SarAr approach,  $5.56 \pm 0.91$  %ID/g in the tumor for  $^{64}\text{Cu}$ -Tz-SarAr at 4 h p.i. compared to  $4.09 \pm 0.61$  for  $^{64}\text{Cu}$ -Tz-NOTA at the same time-point, possibly a consequence of the slightly enhanced stability of  $^{64}\text{Cu}$ -Tz-SarAr. Likewise, the tumor-to-background activity ratios are generally slightly improved for the second generation strategy. At 12 h after injection, for example, the tumor-to-blood and tumor-to-muscle activity ratios for  $^{64}\text{Cu}$ -Tz-SarAr are  $3.1 \pm 0.8$  and  $45.1 \pm 8.6$ , respectively, compared to  $1.8 \pm 0.5$  and  $26.6 \pm 6.6$  with  $^{64}\text{Cu}$ -Tz-NOTA. Without question, however, the biggest difference between the  $^{64}\text{Cu}$ -Tz-SarAr and  $^{64}\text{Cu}$ -Tz-NOTA is the clearance, or lack thereof, of the radiotracer through the GI tract. For example, at 1 h post-injection, the activity concentration of  $^{64}\text{Cu}$ -Tz-NOTA in the large intestine and its contents is  $13.29 \pm 3.15$  %ID/g compared to  $0.21 \pm 0.09$  %ID/g for  $^{64}\text{Cu}$ -Tz-SarAr. This change results in a dramatic shift in the tumor-to-large intestine activity ratios for the two systems: from  $1.44 \pm 0.72$  at 12 h p.i. for  $^{64}\text{Cu}$ -Tz-NOTA to  $33.67 \pm 8.82$  for  $^{64}\text{Cu}$ -Tz-SarAr at the same time point. This is an extremely important result as we consider clinical imaging. There is, of course, a trade-off here: the  $^{64}\text{Cu}$ -Tz-SarAr system exhibits slightly higher activity concentrations in its clearance organs, the kidneys. Yet still, the activity levels produced in the kidneys by  $^{64}\text{Cu}$ -Tz-SarAr are generally well below those produced in the gut by  $^{64}\text{Cu}$ -Tz-NOTA. More importantly, unlike uptake in the large intestine, low levels of residual uptake in the kidneys will not significantly interfere with the clinical imaging of primary colorectal carcinoma.

With a 24 h accumulation interval, the activity concentration of  $^{64}\text{Cu}$ -Tz-SarAr in the tumor reached a relatively high  $5.63 \pm 0.67$  %ID/g at only 1 h p.i. This value increases slightly over the course of the experiment to  $6.74 \pm 1.26$  %ID/g at 12 h and  $7.38 \pm 2.02$  %ID/g at 24 h. These data, combined with the relatively high blood activity values, suggest that while the *majority* of the in vivo ligations are taking place at the tumor, some radioligand is clicking with the antibody in the blood and reaching the tumor thereafter (Supporting Calculations S1 and S2). Rossin et al. have elegantly shown that the fraction of in vivo ligations between tetrazine-based radioligands and TCO-modified antibodies in the blood can be reduced using tetrazine-bearing clearing agents.<sup>40</sup> Yet despite the effectiveness of this method, the use of a clearing agent undeniably adds unwanted scientific and logistical complexity to the system. Therefore, in an attempt to decrease the frequency of click reactions in the blood—and consequently reduce nontarget tissue activity concentrations—using a simpler approach, PET imaging, and biodistribution experiments were conducted using longer accumulation intervals of 48 and 120 h (Figure 6A,B and Figures S15–S20 and Tables S14–S21). Broadly speaking, two trends could be observed. First, the activity concentrations in the tumor are decreased slightly using the longer intervals: for example, from  $5.6 \pm 0.9$  %ID/g at 4 h p.i. using a 24 h interval to  $5.2 \pm 1.4$  %ID/g and  $3.6 \pm 0.7$  %ID/g at the same time-points using 48 and 120 h intervals, respectively (Figure 6C). This makes sense, of course, as the TCO moiety is not infinitely stable to *trans*–*cis* isomerization (and thus inactivation) *in vivo*. Notably, however, in both cases the amount of uptake in the tumor at 1 h postinjection is nearly identical to that at 24 h, suggesting that longer accumulation intervals effectively eliminate click ligations in the blood. Second, the activity concentrations in the blood, and most other tissues, are reduced (Figure 6D). The activity concentration remaining in the blood at 4 h p.i. with

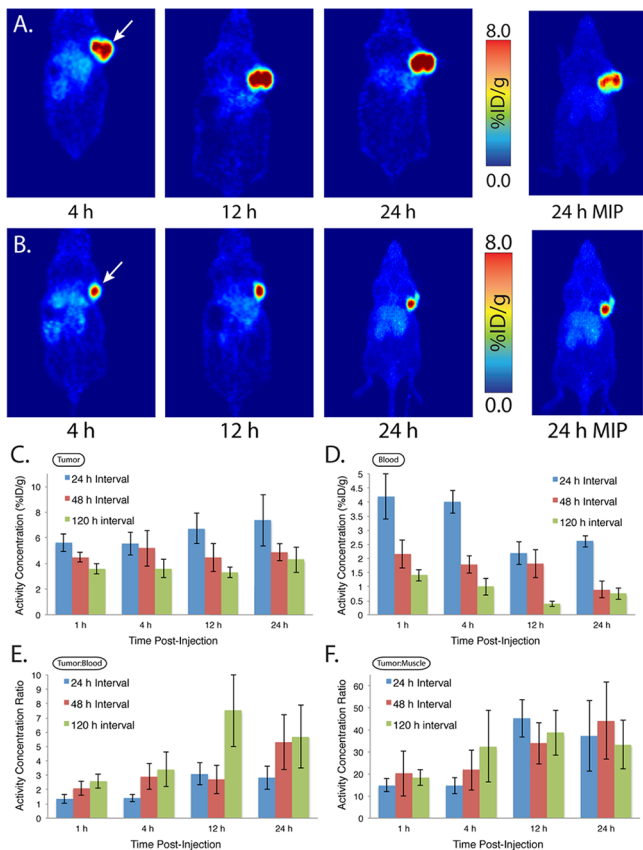


**Figure 6.** (A,B) Pretargeted PET imaging using  $^{64}\text{Cu}$ -Tz-SarAr with 48 h (A) and 120 h (B) accumulation intervals. The coronal slices (left) intersect the center of the tumor (white arrow). Maximum intensity projections (MIP) collected at 24 h postinjection are also displayed (right). (C) Activity concentration in the tumor as a function of both time postinjection and accumulation interval for pretargeting with  $^{64}\text{Cu}$ -Tz-SarAr. (D) Activity concentration in the blood as a function of both time postinjection and accumulation interval for pretargeting with  $^{64}\text{Cu}$ -Tz-SarAr. (E) Tumor-to-blood activity concentration ratios as a function of both time postinjection and accumulation interval for pretargeting with  $^{64}\text{Cu}$ -Tz-SarAr. (F) Tumor-to-muscle activity concentration ratios as a function of both time postinjection and accumulation interval for pretargeting with  $^{64}\text{Cu}$ -Tz-SarAr.

a 24 h accumulation interval is  $4.0 \pm 0.37\% \text{ID/g}$ . Using 48 and 120 h intervals, the corresponding values decrease to  $1.78 \pm 0.28\% \text{ID/g}$  and  $1.05 \pm 0.29\% \text{ID/g}$ , respectively. Taken together, these two trends result in higher tumor-to-blood activity ratios for the longer accumulation intervals: for example,  $2.83 \pm 0.81$ ,  $5.27 \pm 1.92$ , and  $5.74 \pm 2.17$  at 24 h p.i. for 24, 48, and 120 h intervals, respectively (Figure 6E). They do not, however, significantly impact other tumor-to-background activity ratios, as the reductions in nontarget tissue activity concentrations seem to be offset by the decreases in the activity concentrations in the tumor (Figure 6F). Taken together, these data suggest that longer accumulation intervals may be appropriate for pretargeted imaging in the clinical setting.

**Autoradiography and Immunohistochemistry.** Immediately following the pretargeted PET imaging studies, *ex vivo* autoradiographical and immunohistochemical analyses were performed on the SW1222 xenografts in order to learn more about the microscopic distribution of the huA33-TCO and  $^{64}\text{Cu}$ -Tz-SarAr (Figure 7 and Supporting Information Methods).

As expected, hematoxylin and eosin staining of the excised tumors reveals that both huA33-TCO and  $^{64}\text{Cu}$ -Tz-SarAr are almost exclusively associated with tumor cells rather than regions of stromal tissue. More important, however, is the demonstration of the remarkable microscopic colocalization of the autoradiographical signal of  $^{64}\text{Cu}$ -Tz-SarAr and the fluorescence staining for huA33-TCO, an observation which further supports the selective, *in vivo* formation of the completed  $^{64}\text{Cu}$ -SarAr-huA33 radioimmunoconjugate.

**Dosimetry.** The final piece of the puzzle at hand is the investigation of the radiation dosimetry of this pretargeting methodology. After all, the *raison d'être* for any pretargeted approach is the selective delivery of radioisotopes to malignant tissues at radiation doses below those created by traditional radioimmunoconjugates. To this end, dosimetry calculations were performed using the biodistribution data collected and the OLINDA computer program to determine the mean organ absorbed doses (rad/mCi) and effective dose (rem/mCi) for each strategy (Table 2 and Supporting Methods and Table S22).<sup>69</sup> The total effective dose of the  $^{64}\text{Cu}$ -Tz-SarAr pretargeting strategy with a 24 h interval period is 0.041 rem/mCi (0.011 mSv/MBq), a slight reduction compared to the 0.046 rem/mCi (0.012 mSv/MBq) effective dose created by the first generation  $^{64}\text{Cu}$ -Tz-NOTA that can largely be traced to the significant reduction in the mean organ absorbed dose to the large intestine. Not surprisingly given the reduction in the activity concentrations in healthy organs, the total effective dose of the  $^{64}\text{Cu}$ -Tz-SarAr pretargeting strategy is inversely proportional to the duration of the accumulation interval: the dose falls from 0.41 rem/mCi with a 24-h interval to 0.038 rem/mCi (0.010 mSv/MBq) with a 48-h interval and 0.034 rem/mCi (0.009 mSv/MBq) with a 120-h interval. Most important, however, are the dramatic differences between the dosimetry of the  $^{64}\text{Cu}$ -Tz-SarAr pretargeting strategies and directly labeled antibodies. Using a 120-h accumulation interval, the  $^{64}\text{Cu}$ -Tz-SarAr pretargeting approach yields an effective dose of 0.034 rem/mCi, a nearly 4-fold reduction compared to the 0.133 rem/mCi (0.0359 mSv/MBq) effective dose delivered by huA33 labeled directly with  $^{64}\text{Cu}$ . Given the advent of  $^{89}\text{Zr}$ -immunoPET, however, a comparison to the data previously obtained for huA33 directly labeled with  $^{89}\text{Zr}$  is far more clinically relevant. In this case, the effective dose of  $^{89}\text{Zr}$ -DFO-huA33 is 1.54 rem/mCi (0.4162 mSv/MBq), almost 50 times greater than the 0.034 rem/mCi dose associated with  $^{64}\text{Cu}$ -Tz-SarAr pretargeting with a 120-h accumulation interval. Moreover, in some tissues, this dose rate reduction becomes even more pronounced. For example, the mean absorbed doses to osteogenic cells and red marrow with  $^{89}\text{Zr}$ -DFO-huA33 are 6.09 rad/mCi (1.65 mGy/MBq) and 3.12 rad/mCi (0.84 mGy/MBq), respectively, approximately 80 and 120 times higher than the dose delivered to the same tissues by the  $^{64}\text{Cu}$ -Tz-SarAr pretargeting approach.

## CONCLUSIONS

In our initial report of the first generation pretargeted PET imaging strategy, we noted that despite the significant promise of the methodology, the relatively sluggish elimination of the radioligand through the gastrointestinal tract could prove problematic for the rapid clinical imaging of abdominal tumors. Therefore, the ultimate goal of this investigation was clear: the development of a *clinic-ready* strategy for the pretargeted PET imaging of colorectal cancer featuring a tetrazine-bearing radioligand with an improved pharmacokinetic profile. To this

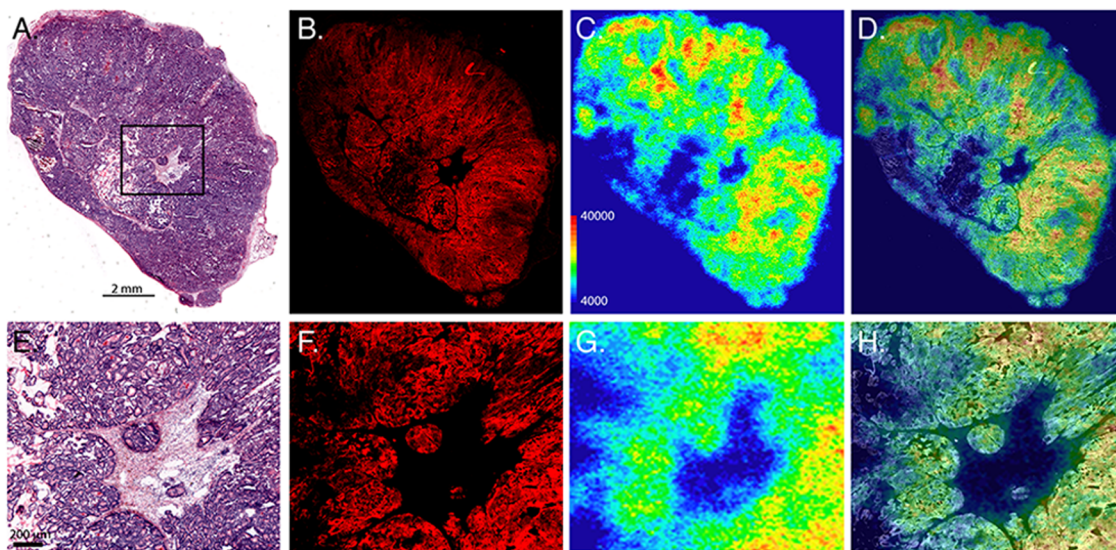


**Figure 7.** Autoradiography, histology, and fluorescence microscopy of SW1222 colorectal carcinoma xenografts resected after pretargeted PET imaging using  $^{64}\text{Cu}$ -Tz-SarAr and an accumulation interval of 120 h. (A) Hematoxylin and eosin staining; (B) immunofluorescence staining for the huA33 antibody; (C) autoradiography indicating the localization of  $^{64}\text{Cu}$ -Tz-SarAr; (D) overlay of immunofluorescence staining and autoradiography; (E) higher magnification image of the area enclosed by the black box in (A); (F–H) higher magnification images of the same area corresponding to (B–D), respectively.

**Table 2. Dosimetry Calculations for Various huA33-Based PET Imaging Strategies**

target organ <sup>a</sup>	$^{89}\text{Zr}$ -DFO-huA33 <sup>b</sup>	$^{64}\text{Cu}$ -NOTA-huA33 <sup>b</sup>	pretargeting				
			$^{64}\text{Cu}$ -Tz-NOTA <sup>b</sup>	24-h interval	24-h interval	48-h interval	120-h interval
adrenals	1.64	0.0726		0.0251	0.0374	0.0347	0.0321
brain	0.764	0.0555		0.0236	0.0364	0.0339	0.0316
breasts	0.621	0.0509		0.0209	0.0325	0.0303	0.0281
gallbladder wall	1.44	0.0741		0.0272	0.0393	0.0368	0.0341
lower lg. int. wall	1.34	0.193		0.166	0.0484	0.0456	0.0400
small intestine	1.11	0.0832		0.033	0.0420	0.0390	0.0362
stomach wall	0.949	0.0883		0.0267	0.0471	0.0385	0.0358
upper lg. int. wall	1.20	0.145		0.114	0.0411	0.0382	0.0355
heart wall	1.55	0.108		0.0294	0.0429	0.0379	0.0329
kidneys	2.53	0.186		0.0315	0.0660	0.0538	0.0565
liver	2.84	0.194		0.0311	0.0301	0.0334	0.0301
lungs	2.26	0.179		0.0289	0.0325	0.0326	0.0215
muscle	1.27	0.0546		0.0138	0.0193	0.0163	0.0139
ovaries	1.09	0.0681		0.0299	0.0404	0.0374	0.0346
pancreas	1.37	0.0708		0.0258	0.0391	0.0362	0.0335
red marrow	3.12	0.308		0.0530	0.0302	0.0280	0.0258
osteogenic cells	6.09	0.439		0.0852	0.0897	0.0805	0.0719
skin	0.677	0.0464		0.0194	0.0298	0.0277	0.0257
spleen	2.52	0.120		0.0180	0.0146	0.0119	0.0112
testes	0.683	0.0522		0.0225	0.0348	0.0322	0.0299
thymus	0.988	0.0584		0.0227	0.0351	0.0325	0.0299
thyroid	0.947	0.0563		0.0228	0.0354	0.0328	0.0303
bladder wall	0.826	0.0609		0.0262	0.0394	0.0365	0.0338
uterus	0.941	0.0652		0.0277	0.0413	0.0382	0.0355
total body	1.39	0.0855		0.0272	0.0380	0.0347	0.0316
effective dose	1.54	0.133		0.046	0.0414	0.0377	0.0339

<sup>a</sup>Mean organ absorbed doses and effective dose are expressed in rad/mCi and rem/mCi, respectively. <sup>b</sup>Data originally reported in Zeglis, B. M. et al. *Journal of Nuclear Medicine*. **54**, 1389–1396 (2013). ©2013 by the Society of Nuclear Medicine and Molecular Imaging. <sup>44</sup>

end, we synthesized two novel radioligands,  $^{64}\text{Cu}$ -Tz-PEG<sub>7</sub>-NOTA and  $^{64}\text{Cu}$ -Tz-SarAr, bearing structural modifications designed to alter their pharmacokinetics. The *in vivo* evaluation of these two constructs revealed that although

$^{64}\text{Cu}$ -Tz-PEG<sub>7</sub>-NOTA is eliminated via both the gastrointestinal and urinary tracts,  $^{64}\text{Cu}$ -Tz-SarAr is cleared through the renal system alone. Pretargeted PET imaging and biodistribution experiments using huA33-TCO,  $^{64}\text{Cu}$ -Tz-SarAr, and mice

bearing human colorectal carcinoma xenografts revealed that this approach delineates malignant tissue with high tumor-to-background contrast at only a fraction of the radiation dose created by traditional, directly labeled radioimmunoconjugates. Of equal importance is that by altering the molecular structure of the tetrazine-bearing radioligand, we were able to effectively eliminate background uptake of the radioligand in the gastrointestinal tract. Given that this approach is intended for the imaging of tumors within the colon, this development is absolutely critical. The clinical translation of this pretargeted PET imaging methodology for the staging, treatment planning, and treatment monitoring of colorectal carcinoma is currently underway at Memorial Sloan Kettering Cancer Center, as well as the further preclinical development of other novel pretargeting methodologies for both imaging and therapy.

## ASSOCIATED CONTENT

### Supporting Information

The Supporting Information is available free of charge on the ACS Publications website at DOI: [10.1021/acs.molpharmaceut.5b00294](https://doi.org/10.1021/acs.molpharmaceut.5b00294).

Reagents and general procedures; detailed experimental methods for chemical syntheses, radiosyntheses, stability assays, in vitro experiments, in vivo experiments, ex vivo histology and autoradiography, and dosimetry calculations; additional PET images; tables of biodistribution data, both absolute activity concentrations and tumor-to-tissue activity concentration ratios; representative calculation of the fraction of in vivo click reactions occurring at the tumor site; representative calculation of the tetrazine/huA33-TCO reaction yield at the tumor site; and dosimetry table using units of mGy/MBq and mSv/MBq ([PDF](#))

## AUTHOR INFORMATION

### Corresponding Authors

\*Address: 413 East 69th Street, New York, New York 10021. Phone: 212-896-0433. Fax: 212-772-5332. E-mail: [brian.zeglis@hunter.cuny.edu](mailto:brian.zeglis@hunter.cuny.edu).

\*Address: 1275 York Avenue, New York, New York 10065. Phone: 646-888-3039. Fax: 646-888-3059. E-mail: [lewisj2@mskcc.org](mailto:lewisj2@mskcc.org).

### Notes

The authors declare no competing financial interest.

## ACKNOWLEDGMENTS

The authors would like to thank Drs. Pat Zanzonico, Steven Larson, Sarah Cheal, and NagaVaraKishore Pillarsetty for their helpful insight, as well as the Ludwig Institute for Cancer Immunotherapy for generously providing the huA33 antibody and SW1222 cells. Technical services provided by the MSKCC Small-Animal Imaging Core Facility, supported in part by NIH Small-Animal Imaging Research Program (SAIRP) Grant No R24 CA83084 and NIH Center Grant No P30 CA08748, are gratefully acknowledged. NIH Shared Instrumentation Grant No 1S10OD012307-01 for the Inveon PET/CT is also gratefully acknowledged. The authors also thank the NIH (Awards 1K99CA178205-01A1 and 4R00CA178205-02; BMZ), the NSF (IGERT 0965983), the Clinical and Translational Science Center (Novel Research and Methodology Seed Funding Award; J.S.L. and B.M.Z.), the Mr. William H. Goodwin and Mrs. Alice Goodwin and the Commonwealth Foundation for Cancer

Research, and the Experimental Therapeutics Center of Memorial Sloan Kettering Cancer Center for their generous funding.

## ABBREVIATIONS

PET, positron emission tomography; IEDDA, inverse electron demand Diels–Alder; Tz, tetrazine; TCO, transcyclooctene; HPLC, high performance liquid chromatography; TLC, thin layer chromatography; DOL, degree of labeling; AF680, AlexaFluor 680; %ID/g, percent injected dose per gram; p.i., postinjection; MIP, maximum intensity projection; NHS, N-hydroxysuccinimide

## REFERENCES

- (1) Wu, A. M. Antibodies and antimatter: The resurgence of immuno-PET. *J. Nucl. Med.* **2009**, *50* (1), 2–5.
- (2) Wu, A. M.; Senter, P. D. Arming antibodies: Prospects and challenges for immunoconjugates. *Nat. Biotechnol.* **2005**, *23* (9), 1137–1146.
- (3) Deri, M. A.; Zeglis, B. M.; Francesconi, L. C.; Lewis, J. S. PET imaging with 89Zr: From radiochemistry to the clinic. *Nucl. Med. Biol.* **2013**, *40* (1), 3–14.
- (4) van Dongen, G. A. M. S.; Visser, G. W. M.; Lub-de Hooge, M. N.; de Vries, E. G.; Perk, L. R. Immuno-PET: a navigator in monoclonal antibody development and applications. *Oncologist* **2007**, *12* (12), 1379–1389.
- (5) Vugts, D. J.; van Dongen, G. A. M. S. 89Zr-labeled compounds for PET imaging guided personalized therapy. *Drug Discovery Today: Technol.* **2011**, *8* (2–4), e53–e61.
- (6) Sharkey, R. M.; Goldenberg, D. M. Cancer radioimmunotherapy. *Immunotherapy* **2011**, *3* (3), 349–370.
- (7) Wu, A. M. Engineered antibodies for molecular imaging of cancer. *Methods* **2014**, *65* (1), 139–147.
- (8) Roovers, R. C.; van Dongen, G. A. M. S.; van Bergen en Henegouwen, P. M. P. Nanobodies in therapeutic applications. *Curr. Opin. Mol. Ther.* **2007**, *9* (4), 327–335.
- (9) Sharkey, R. M.; Chang, C. H.; Rossi, E. A.; McBride, W. J.; Goldenberg, D. M. Pretargeting: Taking an alternate route for localizing radionuclides. *Tumor Biol.* **2012**, *33*, 591–600.
- (10) Goldenberg, D. M.; Chang, C. H.; Rossi, E. A.; McBride, W. J.; Sharkey, R. M. Pretargeted molecular imaging and radioimmunotherapy. *Theranostics* **2012**, *2* (5), 523–540.
- (11) Boerman, O. C.; van Schaijk, F. G.; Oyen, W. J. G.; Corstens, F. H. M. Pretargeted radioimmunotherapy of cancer: Progress step by step. *J. Nucl. Med.* **2003**, *44* (3), 400–411.
- (12) Sharkey, R. M.; Goldenberg, D. M. Advances in radioimmunotherapy in the age of molecular engineering and pretargeting. *Cancer Invest.* **2006**, *24* (1), 82–97.
- (13) Lewis, M. R.; Wang, M.; Axworthy Donald, B.; Theodore Louis, J.; Mallet Robert, W.; Fritzberg Alan, R.; Welch Michael, J.; Anderson Carolyn, J. In vivo evaluation of pretargeted 64Cu for tumor imaging and therapy. *J. Nucl. Med.* **2003**, *44* (8), 1284–92.
- (14) Goldenberg, D. M.; Sharkey, R. M.; Paganelli, G.; Barbet, J.; Chatal, J. F. Antibody pretargeting advances cancer radioimmuno-detection and radioimmunotherapy. *J. Clin. Oncol.* **2006**, *24* (5), 823–834.
- (15) Cauchon, N.; Langlois, R.; Rousseau, J. A.; Tessier, G.; Cadorette, J.; Lecomte, R.; Hunting, D. J.; Pavan, R. A.; Zeisler, S. K.; van Lier, J. E. PET imaging of apoptosis with Cu-64-labeled streptavidin following pretargeting of phosphatidylserine with biotinylated annexin-V. *Eur. J. Nucl. Med. Mol. Imaging* **2007**, *34* (2), 247–258.
- (16) Liu, G.; Mang'era, K.; Liu, N.; Gupta, S.; Rusckowski, M.; Hnatowich, D. Tumor pretargeting in mice using 99mTc-labeled morpholino, a DNA analog. *J. Nucl. Med.* **2002**, *43*, 384–391.
- (17) Liu, G.; Dou, S.; Liu, Y.; Wang, Y.; Rusckowski, M.; Hnatowich, D. J. 90Y-labeled Phosphorodiamidate Morpholino Oligomer for Pretargeting Radiotherapy. *Bioconjugate Chem.* **2011**, *22* (12), 2539–2545.

- (18) Goldenberg, D. M.; Rossi, E. A.; Sharkey, R. M.; McBride, W. J.; Chang, C. H. Multifunctional antibodies by the dock-and-lock method for improved cancer Imaging and therapy by pretargeting. *J. Nucl. Med.* **2008**, *49* (1), 158–163.
- (19) Hollander, N. Bispecific antibodies for cancer therapy. *Immunotherapy* **2009**, *1* (2), 211–222.
- (20) Schoffelen, R.; Sharkey, R. M.; Goldenberg, D. M.; Franssen, G.; McBride, W. J.; Rossi, E. A.; Chang, C. H.; Laverman, P.; Disselhorst, J. A.; Eek, A.; van der Graaf, W. T. A.; Oyen, W. J. G.; Boerman, O. C. Pretargeted immuno-positron emission tomography imaging of carcinoembryonic antigen-expressing tumors with a bispecific antibody and a Ga-68- and F-18-labeled hapten peptide in mice with human tumor xenografts. *Mol. Cancer Ther.* **2010**, *9* (4), 1019–1027.
- (21) Orcutt, K. D.; Rhoden, J. J.; Ruiz-Yi, B.; Frangioni, J. V.; Wittrup, K. D. Effect of small-molecule–binding affinity on tumor uptake in vivo: A systematic study using a pretargeted bispecific antibody. *Mol. Cancer Ther.* **2012**, *11*, 1365.
- (22) Corneillie, T. M.; Lee, K. C.; Whetstone, P. A.; Wong, J. P.; Meares, C. F. Irreversible engineering of the multielement-binding antibody 2D12.5 and its complementary ligands. *Bioconjugate Chem.* **2004**, *15* (6), 1392–1402.
- (23) Reiner, T.; Zeglis, B. M. The inverse electron demand Diels-Alder reaction in radiochemistry. *J. Labelled Compd. Radiopharm.* **2014**, *57*, 285–290.
- (24) Blackman, M. L.; Royzen, M.; Fox, J. M. Tetrazine ligation: fast bioconjugation based on inverse electron demand Diels-Alder reactivity. *J. Am. Chem. Soc.* **2008**, *130*, 13518–13519.
- (25) Li, Z.; Cai, H.; Hassink, M.; Blackman, M.; Brown, R. C. D.; Conti, P. S.; Fox, J. M. Tetrazine-trans-cyclooctene ligation for the rapid construction of 18-F labeled probes. *Chem. Commun.* **2010**, *46*, 8043–8045.
- (26) Selvaraj, R.; Liu, S. L.; Hassink, M.; Huang, C. W.; Yap, L. P.; Park, R.; Fox, J. M.; Li, Z. B.; Conti, P. S. Tetrazine-trans-cyclooctene ligation for the rapid construction of integrin alpha(v)beta(3) targeted PET tracer based on a cyclic RGD peptide. *Bioorg. Med. Chem. Lett.* **2011**, *21* (17), 5011–5014.
- (27) Liu, S.; Hassink, M.; Selvaraj, R.; Yap, L. P.; Park, R.; Wang, H.; Chen, X.; Fox, J. M.; Li, Z.; Conti, P. S. Efficient 18F labeling of cysteine-containing peptides and proteins using tetrazine-trans-cyclooctene ligation. *Molecular Imaging* **2013**, *12*, 121–128.
- (28) Zeglis, B. M.; Mohindra, P.; Weissmann, G. I.; Divilov, V.; Hilderbrand, S. A.; Weissleder, R.; Lewis, J. S. Modular strategy for the construction of radiometalated antibodies for positron emission tomography based on inverse electron demand Diels-Alder click chemistry. *Bioconjugate Chem.* **2011**, *22* (10), 2048–2059.
- (29) Emmetiere, F.; Irwin, C.; Viola-Villegas, N. T.; Longo, C. A.; Cheal, S. M.; Zanzonico, P.; Weber, W. A.; Lewis, J. S.; Reiner, T. 18F-labeled-bioorthogonal liposomes for in vivo targeting. *Bioconjugate Chem.* **2013**, *24*, 1784–1789.
- (30) Zeglis, B. M.; Emmetiere, F.; Pillarsetty, N.; Weissleder, R.; Lewis, J. S.; Reiner, T. Building blocks for the construction of bioorthogonally reactive peptides via solid-phase peptide synthesis. *ChemistryOpen* **2014**, *3* (2), 48–53.
- (31) Reiner, T.; Lacy, J.; Keliher, E. J.; Yang, K. S.; Ullal, A.; Kohler, R. H.; Vinegoni, C.; Weissleder, R. Imaging therapeutic PARP inhibition in vivo through bioorthogonally developed companion imaging agents. *Neoplasia* **2012**, *14*, 169–177.
- (32) Devaraj, N. K.; Upadhyay, R.; Hatin, J. B.; Hilderbrand, S. A.; Weissleder, R. Fast and sensitive pretargeted labeling of cancer cells through a tetrazine/trans-cyclooctene cycloaddition. *Angew. Chem., Int. Ed.* **2009**, *48* (38), 7013–7016.
- (33) Devaraj, N. K.; Hilderbrand, S.; Upadhyay, R.; Mazitschek, R.; Weissleder, R. Bioorthogonal turn-on probes for imaging small molecules inside living cells. *Angew. Chem., Int. Ed.* **2010**, *49*, 2869–2872.
- (34) Han, H. S.; Devaraj, N. K.; Lee, J.; Hilderbrand, S.; Weissleder, R.; Bawendi, M. G. Development of a bioorthogonal and highly efficient conjugation method for quantum dots using tetrazine-norbornene cycloaddition. *J. Am. Chem. Soc.* **2010**, *132*, 7838–7839.
- (35) Haun, J. B.; Devaraj, N. K.; Hilderbrand, S.; Lee, H.; Weissleder, R. Bioorthogonal chemistry amplifies nanoparticle binding and enhances the sensitivity of cell detection. *Nat. Nanotechnol.* **2010**, *5*, 660–665.
- (36) Karver, M. R.; Weissleder, R.; Hilderbrand, S. A. Synthesis and evaluation of a series of 1,2,4,5-tetrazines for bioorthogonal conjugation. *Bioconjugate Chem.* **2011**, *22* (11), 2263–2270.
- (37) Devaraj, N. K.; Weissleder, R. Biomedical applications of tetrazine cycloadditions. *Acc. Chem. Res.* **2011**, *44*, 816–827.
- (38) Rossin, R.; van den Bosch, S. M.; Ten Hoeve, W.; Carvelli, M.; Versteegen, R. M.; Lub, J.; Robillard, M. S. Highly reactive trans-cyclooctene tags with improved stability for Diels-Alder chemistry in living systems. *Bioconjugate Chem.* **2014**, *34*, 1210–1217.
- (39) Rossin, R.; Verkerk, P. R.; van den Bosch, S. M.; Vulders, R. C. M.; Verel, I.; Lub, J.; Robillard, M. S. In vivo chemistry for pretargeted tumor imaging in live mice. *Angew. Chem., Int. Ed.* **2010**, *49*, 3375–3378.
- (40) Rossin, R.; Lappchen, R.; van den Bosch, S. M.; LaForest, R.; Robillard, M. S. Diels-Alder reaction for tumor pretargeting: In vivo chemistry can boost tumor radiation dose compared with directly labeled antibody. *J. Nucl. Med.* **2013**, *54*, 1989–1995.
- (41) Devaraj, N. K.; Thurber, G. M.; Keliher, E. J.; Marinelli, B.; Weissleder, R. Reactive polymer enables efficient in vivo bioorthogonal chemistry. *Proc. Natl. Acad. Sci. U. S. A.* **2012**, *109* (13), 4762–4767.
- (42) Nichols, B.; Qin, Z. T.; Yang, J.; Vera, D. R.; Devaraj, N. K. Ga-68 chelating bioorthogonal tetrazine polymers for the multistep labeling of cancer biomarkers. *Chem. Commun.* **2014**, *50* (40), 5215–5217.
- (43) Evans, H. L.; Nguyen, Q. D.; Carroll, L. S.; Kaliszczak, M.; Twyman, F. J.; Spivey, A. C.; Aboagye, E. O. A bioorthogonal Ga-68 labelling strategy for rapid in vivo imaging. *Chem. Commun.* **2014**, *50* (67), 9557–9560.
- (44) Zeglis, B. M.; Sevak, K. K.; Reiner, T.; Mohindra, P.; Carlin, S.; Zanzonico, P.; Weissleder, R.; Lewis, J. S. A pretargeted PET imaging strategy based on bioorthogonal Diels-Alder click chemistry. *J. Nucl. Med.* **2013**, *54*, 1389–1396.
- (45) McCarthy, D. W.; Shefer, R. E.; Klinkowstein, R. E.; Bass, L. A.; Margeneau, W. H.; Cutler, C. S.; Anderson, C. J.; Welch, M. J. Efficient production of high specific activity <sup>64</sup>Cu using a biomedical cyclotron. *Nucl. Med. Biol.* **1997**, *24* (1), 35–43.
- (46) Kume, M.; Carey, P. C.; Gaehle, G.; Madrid, E.; Voller, T.; Margenau, W.; Welch, M. J.; Lapi, S. E. A semi-automated system for the routine production of copper-64. *Appl. Radiat. Isot.* **2012**, *70* (8), 1803–1806.
- (47) Sakamoto, J.; Kojima, H.; Kato, J.; Hamashima, H.; Suzuki, H. Organ-specific expression of the intestinal epithelium-related antigen A33, a cell surface target for antibody-based imaging and treatment in gastrointestinal cancer. *Cancer Chemother. Pharmacol.* **2000**, *46*, S27–S32.
- (48) Welt, S.; Scott, A. M.; Divgi, C. R.; Kemeny, N. E.; Finn, R. D.; Daghigian, F.; StGermain, J.; Richards, E. C.; Larson, S. M.; Old, L. J. Phase I/II study of iodine 125-labeled monoclonal antibody A33 in patients with advanced colon cancer. *J. Clin. Oncol.* **1996**, *14* (6), 1787–1797.
- (49) Sakamoto, J.; Oriuchi, N.; Mochiki, E.; Asao, T.; Scott, A. M.; Hoffman, E. W.; Jungbluth, A. A.; Matsui, T.; Lee, F. T.; Papenfuss, A.; Kuwano, H.; Takahashi, T.; Endo, K.; Old, L. J. A phase I radioimmunolocalization trial of humanized monoclonal antibody huA33 in patients with gastric carcinoma. *Cancer Sci.* **2006**, *97* (11), 1248–1254.
- (50) Scott, A. M.; Lee, F. T.; Jones, R.; Hopkins, W.; MacGregor, D.; Cebon, J. S.; Hannah, A.; Chong, G.; U, P.; Papenfuss, A.; Rigopoulos, A.; Sturrock, S.; Murphy, R.; Wirth, V.; Murone, C.; Smyth, F. E.; Knight, S.; Welt, S.; Ritter, G.; Richards, E.; Nice, E. C.; Burgess, A. W.; Old, L. J. A phase I trial of humanized monoclonal antibody A33 in patients with colorectal carcinoma: Biodistribution, pharmacokinetics, and quantitative tumor uptake. *Clin. Cancer Res.* **2005**, *11* (13), 4810–4817.
- (51) Carrasquillo, J. A.; Pandi-Taskar, N.; O'Donoghue, J. A.; Humm, J. L.; Zanzonico, P.; Smith-Jones, P. M.; Divgi, C. R.; Pryma, D. A.; Ruan, S.; Kemeny, N. E.; Fong, Y.; Wong, D.; Jaggi, J. S.; Scheinberg, D. A.;

- Gonen, M.; Panageas, K. S.; Ritter, G.; Jungbluth, A. A.; Old, L. J.; Larson, S. M. 124I-huA33 antibody PET of colorectal cancer. *J. Nucl. Med.* **2011**, *52* (8), 1173–1180.
- (52) Ackerman, M. E.; Chalouni, C.; Schmidt, M. M.; Raman, V. V.; Ritter, G.; Old, L. J.; Mellman, I.; Wittrup, K. D. A33 antigen displays persistent surface expression. *Cancer Immunol. Immunother.* **2008**, *57*, 1017–1027.
- (53) Shi, J.; Jin, Z.; Liu, X.; Fan, D.; Sun, Y.; Zhao, H.; Zhu, Z.; Liu, Z.; Jia, B.; Wang, F. PET imaging of neovascularization with Ga-68-3PRGD(2) for assessing tumor early response to endostar antiangiogenic therapy. *Mol. Pharmaceutics* **2014**, *11* (11), 3915–3922.
- (54) Leyton, J.; Iddon, L.; Perumal, M.; Indrevoll, B.; Glaser, M.; Robins, E.; George, A. J. T.; Cuthbertson, A.; Luthra, S. K.; Aboagye, E. O. Targeting somatostatin receptors: preclinical evaluation of novel F-18-fluoroethyltriazole-Tyr(3)-octreotate analogs for PET. *J. Nucl. Med.* **2011**, *52* (9), 1441–1448.
- (55) Hausner, S. H.; Carpenter, R. D.; Bauer, N.; Sutcliffe, J. L. Evaluation of an integrin alpha(v)beta(6)-specific peptide labeled with [F-18]fluorine by copper-free, strain-promoted click chemistry. *Nucl. Med. Biol.* **2013**, *40* (2), 233–239.
- (56) Hausner, S. H.; Bauer, N.; Sutcliffe, J. L. In vitro and in vivo evaluation of the effects of aluminum [F-18]fluoride radiolabeling on an integrin alpha(v)beta(6)-specific peptide. *Nucl. Med. Biol.* **2014**, *41* (1), 43–50.
- (57) Guo, J.; Lang, L.; Hu, S.; Guo, N.; Zhu, L.; Sun, Z.; Ma, Y.; Kiesewetter, D. O.; Niu, G.; Xie, Q.; Chen, X. Comparison of three dimeric F-18-AlF-NOTA-RGD tracers. *Mol. Imag. Biol.* **2014**, *16* (2), 274–283.
- (58) Fournier, P.; Dumulon-Perreault, V.; Ait-Mohand, S.; Tremblay, S.; Benard, F.; Lecomte, R.; Guerin, B. Novel radiolabeled peptides for breast and prostate tumor PET imaging: Cu-64/and Ga-68/NOTA-PEG-[D-Tyr(6),beta Ala(11),Thi(13),Nle(14)]BBN(6–14). *Bioconjugate Chem.* **2012**, *23* (8), 1687–1693.
- (59) Anderson, C. J.; Pajean, T. S.; Edwards, W. B.; Sherman, E. L. C.; Rogers, B. E.; Welch, M. J. In vitro and in vivo evaluation of copper-64-octreotide conjugates. *J. Nucl. Med.* **1995**, *36* (12), 2315–2325.
- (60) Cai, Z.; Ouyang, Q.; Zeng, D.; Nguyen, K. N.; Modi, J.; Wang, L.; White, A. G.; Rogers, B. E.; Xie, X.-Q.; Anderson, C. J. Cu-64-labeled somatostatin analogues conjugated with cross-bridged phosphonate-based chelators via strain-promoted click chemistry for PET imaging: In silico through in vivo studies. *J. Med. Chem.* **2014**, *57* (14), 6019–6029.
- (61) Dearling, J. L. J.; Paterson, B. M.; Akurathi, V.; Betanzos-Lara, S.; Treves, S. T.; Voss, S. D.; White, J. M.; Huston, J. S.; Smith, S. V.; Donnelly, P. S.; Packard, A. B. The ionic charge of copper-64 complexes conjugated to an engineered antibody affects biodistribution. *Bioconjugate Chem.* **2015**, *26*, 707.
- (62) Garcia Garayoa, E.; Schweinsberg, C.; Maes, V.; Brans, L.; Blauenstein, P.; Tourwe, D. A.; Schibli, R.; Schubiger, P. A. Influence of the molecular charge on the biodistribution of bombesin analogues labeled with the [99mTc(CO)3]-core. *Bioconjugate Chem.* **2008**, *19* (12), 2409–16.
- (63) Lewis, J. S.; Lewis, M. R.; Srinivasan, A.; Schmidt, M. A.; Wang, J.; Anderson, C. J. Comparison of four Cu-64-labeled somatostatin analogues in vitro and in a tumor-bearing rat model: Evaluation of new derivatives for positron emission tomography imaging and targeted radiotherapy. *J. Med. Chem.* **1999**, *42* (8), 1341–1347.
- (64) Notni, J.; Pohle, K.; Wester, H.-J. Comparative gallium-68 labeling of TRAP-, NOTA-, and DOTA-peptides: Practical consequences for the future of gallium-68-PET. *EJNMMI Res.* **2012**, *2* (1), 28–28.
- (65) Rahim, M. K.; Kota, R.; Haun, J. B. Enhancing reactivity for bioorthogonal pretargeting by unmasking antibody-conjugated trans-cyclooctenes. *Bioconjugate Chem.* **2015**, *26* (2), 352–360.
- (66) Varasteh, Z.; Mitran, B.; Rosenstrom, U.; Velikyan, I.; Rosestedt, M.; Lindeberg, G.; Sorensen, J.; Larhed, M.; Tolmachev, V.; Orlova, A. The effect of macrocyclic chelators on the targeting properties of the Ga-68-labeled gastrin releasing peptide receptor antagonist PEG(2)-RM26. *Nucl. Med. Biol.* **2015**, *42* (5), 446–454.
- (67) Tsiafa, I.; Loudos, G.; Varvarigou, A.; Fragogeorgi, E.; Psimadas, D.; Tsotakos, T.; Xanthopoulos, S.; Mihailidis, D.; Bouziotis, P.; Nikiforidis, G. C.; Kagadis, G. C. Biological evaluation of an ornithine-modified Tc-99m-labeled RGD peptide as an angiogenesis imaging agent. *Nucl. Med. Biol.* **2013**, *40* (2), 262–272.
- (68) Antunes, P.; Ginj, M.; Walter, M. A.; Chen, J. H.; Reubi, J. C.; Maecke, H. R. Influence of different spacers on the biological profile of a DOTA-somatostatin analogue. *Bioconjugate Chem.* **2007**, *18* (1), 84–92.
- (69) Stabin, M. G.; Sarks, R. B.; Crowe, E. OLINDA/EXM: The second-generation personal computer software for internal dose assessment in nuclear medicine. *J. Nucl. Med.* **2005**, *45* (6), 1023–1027.